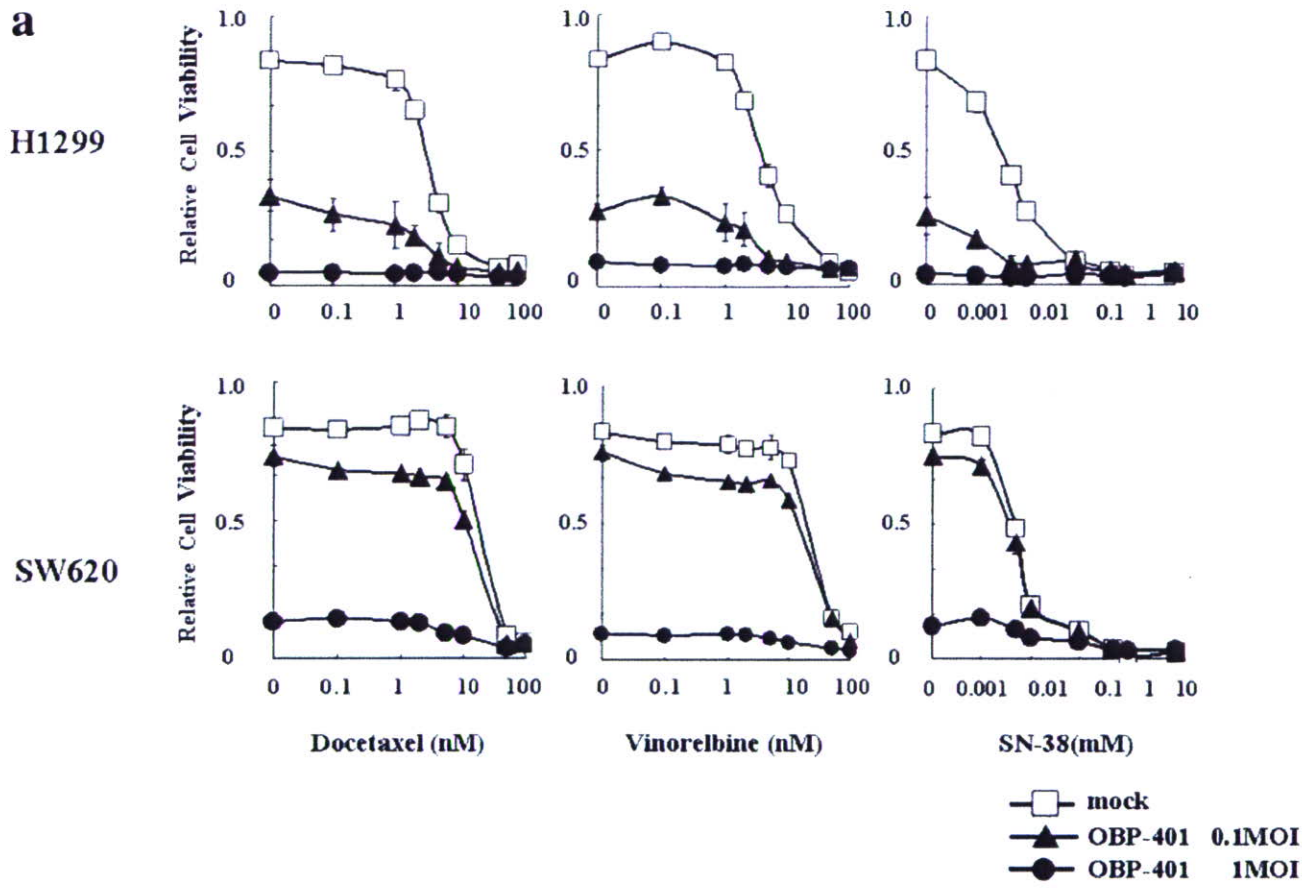

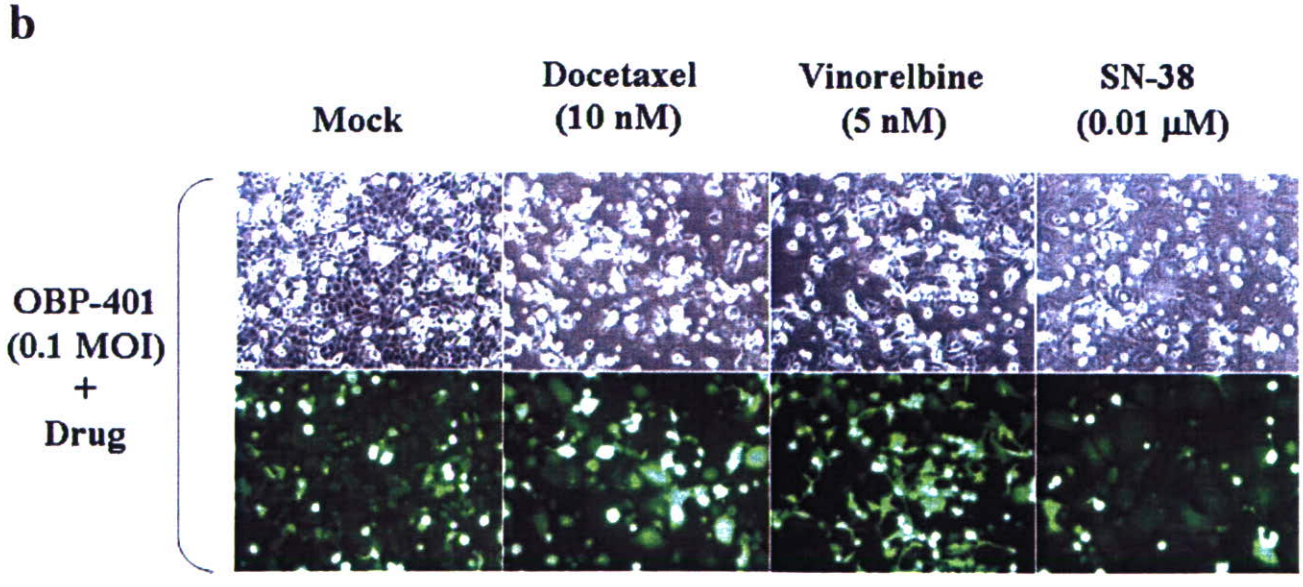

FIGURE 3 – Combination efficacy of OBP-401 with other chemotherapeutic agents, the topoisomerase I inhibitor SN-38 (active irinotecan metabolite) and microtubule-interfering agent vinorelbine. (*a*) H1299 and SW620 cells were infected with 0.1 or 1 MOI of OBP-401, and then exposed to docetaxel, vinorelbine or SN-38 at the indicated concentrations 24 hr after infection. Cell viability was assessed by XTT assay 5 days after OBP-401 infection. Data are mean ± SD. (*b*) H1299 cells were treated with OBP-401 alone or in combination with drugs (docetaxel [10 nM], vinorelbine [5 nM] or SN-38 [0.01 μM]) according to the schedule described above, and photographed 4 days after OBP-401 infection. Upper panel: phase-contrast images; lower panel: fluorescent images for GFP expression. ×100 magnification.

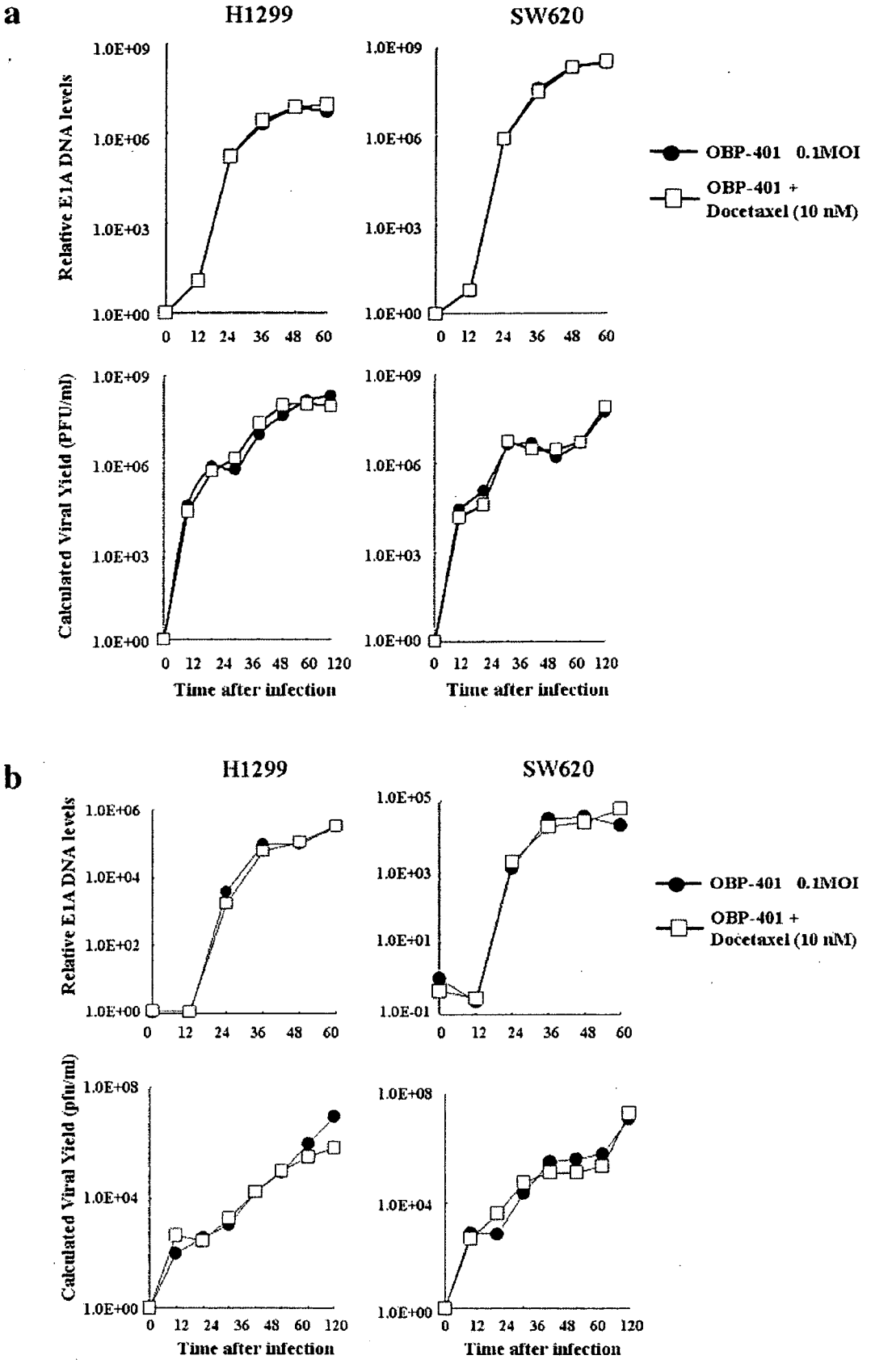

FIGURE 4 – Assessment of viral DNA replication in H1299 and SW620 cells. (*a*) Cells were infected with OBP-401 at an MOI of 0.1 for 2 hr. Following the removal of virus inocula, the cells were further incubated with docetaxel for indicated periods of time. (*b*) Alternatively, cells were treated with docetaxel, followed by 0.1 MOI of OBP-401 infection 24 hr later. Cells (upper panels) and culture supernatants (lower panels) were then subjected to real-time quantitative PCR assay. The amounts of viral E1A copy number are defined as the fold increase for each sample relative to that at 2 hr (2 hr equals 1).

tivity of docetaxel, especially at low concentrations (<10 nM), in most of cell lines, including H1299, SW620, DLD-1, A549, MKN28 and TE8, although OBP-401 at an MOI of 1 alone showed an apparent cell killing activity in these cell lines. In contrast, the effect of the combination was unclear in HepG2, LNCaP, H226Br and T.Tn cell lines, since HepG2 and LNCaP cells were too sensitive and H226Br and T.Tn cells were too resistant to OBP-401. The representative dose–response curves on H1299, HepG2 and T.Tn cells were shown in Figure 2*a*.

We next performed a time-course analysis of the cell killing effect of 0.1 MOI of OBP-401 combined with 10 nM of docetaxel in H1299 and SW620 cells. The viability of cells treated with both agents was consistently lower than that of cells treated with either drug alone over 6 days (Fig. 2*b*). To determine whether the timing of administration of the tested agents affected the combined cytotoxic effect, H1299 and SW620 cells were treated with docetaxel 24 hr before infection, after infection or synchronously with OBP-401. The results showed no apparent differences in the cytotoxic activity of the schedules (data not shown).

Effect of vinorelbine and SN-38 on OBP-401-mediated antitumor activity in human cancer cells in vitro

We also examined the interactive effects of OBP-401 when combined with other chemotherapeutic agents such as the topoisomerase I inhibitor, SN-38 (the active irinotecan metabolite), and a microtubule-interfering agent, vinorelbine, in H1299 and SW620 cells. As shown in Figure 3*a*, the profile of the cytotoxic effects of OBP-401 plus vinorelbine was similar to that of OBP-401 plus docetaxel, whereas the range of combination effectiveness was narrow when combined with SN-38. The combined effect of OBP-401 plus SN38 diminished with the use of high concentrations of SN38, suggesting that inhibition of DNA synthesis may be deleterious for viral replication.

One of the advantages of OBP-401 over OBP-301 is that the viral distribution of OBP-401 can be monitored by GFP fluorescence. With time, infected cells fluoresce in green color, and they expand, float and gather in the center of the well. To confirm visually the viral replication and spread following OBP-401 application, H1299 cells were treated with OBP-401 at an MOI of 0.1 plus 10 nM docetaxel, 5 nM vinorelbine or 0.01 μM SN-38. Phase-contrast images demonstrated growth of H1299 cells to subconfluence in the presence of the chemotherapeutic drugs alone 4 days after treatment, whereas a rapid loss of viability due to massive cell death, as evidenced by ballooning and floating cells, was evident when combined with OBP-401 infection (Fig. 3*b*). A strong and persistent GFP fluorescence expression, which indicates the viral replication and spread into the neighboring tumor cells, was detectable in H1299 cells infected with OBP-401 under a fluorescence microscope even in the presence of chemotherapeutic drugs. The signal intensity of cells treated with OBP-401 plus docetaxel or vinorelbine was equivalent to that of cells infected with OBP-401 alone, whereas the levels of GFP expression was relatively weak in cells treated with OBP-401 and SN-38.

Effect of docetaxel on OBP-401 virus replication in human cancer cells in vitro

We next examined the effect of docetaxel on replication and release of viral progenies by quantitative real-time PCR analysis. H1299 and SW620 cells were infected with OBP-401 at an MOI of 0.1 for 24 hr, and then treated with 10 nM of docetaxel. Alternatively, cells were treated with docetaxel at 10 nM, and then infected with 0.1 MOI of OBP-401 24 hr later. The cells and supernatants were harvested at indicated time points over 60 or 120 hr after infection, and extracted DNA was subjected to the assay. As shown in Figure 4, the increases of intracellular and supernatant viral copy numbers of OBP-401 by 5–9 orders of magnitude were consistent with and without docetaxel over time in both treatment regimens. A plateau was reached at ~48 hr after infection. These results suggest that docetaxel does not interfere with OBP-401 replication.

Antitumor effect of OBP-401 plus docetaxel in human tumor xenografts

Finally, we assessed the therapeutic efficacy of OBP-401 in combination with docetaxel against H1299 human cells *in vivo*. H1299 cells were implanted as xenografts into the hind flank of *nu/nu* mice. Mice bearing palpable H1299 tumors measuring 5–10 mm in diameter received simultaneous treatment of intratumoral injection of either 10^7 PFU of OBP-401 or PBS plus intraperitoneal administration of either 12.5 mg/kg docetaxel or PBS every 2 days for 3 cycles starting at day 1. As shown in Figure 5, administration of OBP-401 or docetaxel resulted in a significant tumor growth suppression compared with mock-treated tumors at 27 days after initiation of treatment ($p < 0.05$). However, the combination of OBP-401 plus docetaxel produced a more profound and significant inhibition of tumor growth compared with mice treated with either modality ($p < 0.05$), and mock-treated tumors ($p < 0.01$). Intratumoral injection of a replication-deficient adenovirus with or without systemic administration of docetaxel had no apparent effect on the growth of H1299 tumors (data not shown).

To investigate the mechanism of action of these therapies and their influence on other body tissues, mice were sacrificed 6 days after the last administration of 10^7 PFU of OBP-401 and 12.5 mg/kg docetaxel. Fluorescent images of frozen sections demonstrated that intratumorally administered OBP-401 spread throughout the tumors whether combined with docetaxel or not, whereas no GFP-expressing cells were detected in the liver tissues (Fig. 6*a*). The broad virus distribution in the tumor was also confirmed by immunohistochemical staining of adenoviral hexon protein (data not shown). Histopathological analysis revealed massive degeneration of tissues, especially in the central portions of tumors injected with OBP-401, but not in those treated with docetaxel alone (Fig. 6*b*). In contrast, analysis of liver sections from mice treated with OBP-401 demonstrated no histological evidence of hepatocellular damage.

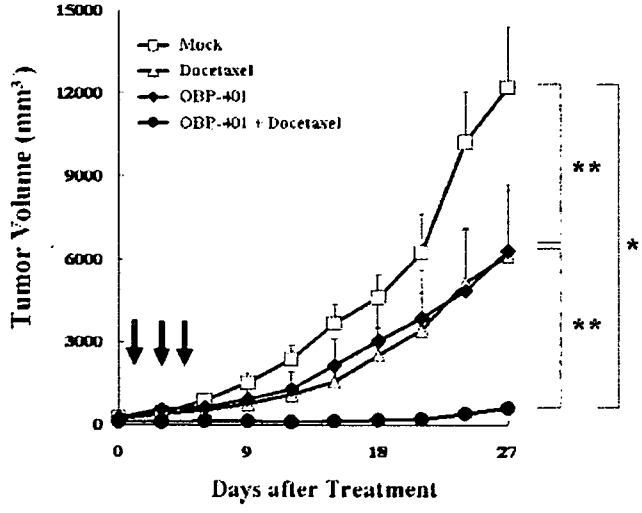

FIGURE 5 – Antitumor effects of intratumorally injected OBP-401and intraperitoneally administered docetaxel against established flank H1299 xenograft tumors in *nu/nu* mice. H1299 tumor cells (1×10^7 cells/each) were subcutaneously injected into the right flank of mice. OBP-401 (1×10^7 PFU/body) and docetaxel (12.5 mg/kg) were administered intratumorally and intraperitoneally, respectively, for 3 cycles every 2 days. PBS was used as the control. Six mice were used for each group. Tumor growth was expressed by tumor mean volume ± SE. Statistical significance was defined as $p < 0.01$ (*) or $p < 0.05$ (**) (Student's *t*-test). Arrows, day of treatment.

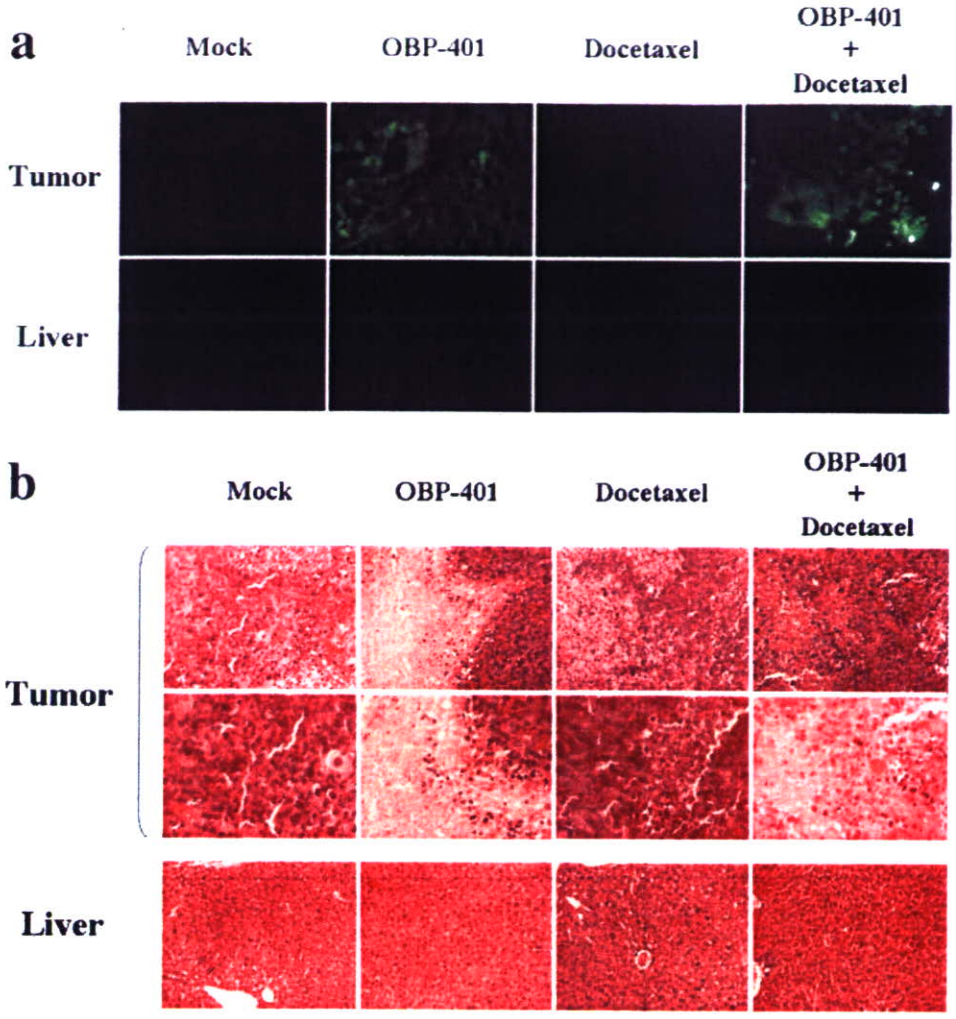

FIGURE 6 – Mice bearing H1299 xenografts were treated as described in the legend for Figure 5. Tumor and liver sections were then obtained 6 days after final administration of OBP-401 and docetaxel. (*a*) Fluorescent photomicrographs showing GFP expression in H1299 tumors and the liver. Magnification, ×200. (*b*) Paraffin sections of tumors and the liver were stained with hematoxylin and eosin. Tumors: (upper panel) magnification, ×200. (lower panel) magnification, ×400. Livers: magnification, ×200.

Discussion

Treatment of advanced human cancer has not significantly improved clinical outcome. Replication-competent oncolytic adenovirus is promising as a novel anticancer therapy.[5–9] In our laboratory, the tumor-specific replication-selective adenovirus, named Telomelysin or OBP-301, has been shown to be effective against human cancers.[10–12] This virus was genetically designed to replicate under the control of hTERT promoter specifically in tumor cells, causing specific "oncolysis." Therefore, OBP-301 did not cause significant toxicity in normal human cell lines, as shown in our previous report.[10–12] In humans, telomerase activity is found in only few cell types like stem and germ-line cells. Thus, there is concern that these cells might be permissive for OBP-301 replication; these cells, however, are not of epithelial origin and are therefore extremely difficult to be targeted with adenoviral vectors.[20]

Preclinical studies provided experimental evidence for effective killing of cancer cells by oncolytic viruses.[5–9] In animal models, however, established xenograft tumors are rarely eliminated despite existence of persistently high viral titers within the tumor. Total elimination of solid tumor requires higher doses of oncolytic viruses, which might be toxic or lethal. In a report of clinical trial of ONYX-015, no clinical benefit was noted in the majority of patients, despite the encouraging biological activity.[21] Tumor progression was rapid in most patients, even though substantial necrosis was noted in the tumors after treatment.[22,23] Therefore, we searched for new modalities and opted to evaluate chemovirotherapy, composed of oncolytic virotherapy combined with low-dose chemotherapeutic agent. Combination of 2 agents may allow the use of reduced dosage of each agent, and reduce the likelihood of adverse effects.

The efficacy of virotherapy combined with anticancer drugs has been reported previously in preclinical studies.[24–26] A replication-selective adenovirus, ONYX-015, combined with 5-fluorouracil or CDDP produced greater effect than each individual modality and prolonged survival.[24,25] Furthermore, synergistic efficacy was also observed in the combination of a tumor-specific HSV mutant (HSV-1716) with chemotherapeutic agents in human non-small cell lung cancer.[26] However, care should be taken when using a combination of anti-DNA synthetic agents because they might have deleterious effects on viral replication. Because adenoviral E1A directs the progression cells from G1/G0 phase to S phase to optimize viral DNA replication, these agents could harm this function by inhibiting DNA synthesis.

Taxanes are novel antimicrotubule agents that promote the assembly of microtubules from tubulin dimers and stabilize microtubules by preventing depolymerization. This stability results in the inhibition of the normal dynamic reorganization of the microtubule network, which is essential for vital interphase and mitotic cellular functions, resulting in cell arrest in G2 and M phases.[17,18] Apoptotic cell death is induced subsequently, but this does not inhibit DNA synthesis of host cells. Therefore, taxanes are promising for combination with virotherapy. It was reported previously

that paclitaxel had a synergistic or an additive effect in several cancer models when combined with Ad-mediated p53 gene therapy.[27] It has been also demonstrated that CV787, a prostate cancer-specific adenovirus, exhibited synergistic antitumor effect when combined with paclitaxel or docetaxel.[28]

OBP-401, containing the hTERT promoter-driven replication cassette and the GFP gene driven by the CMV promoter, was developed to monitor replication and visualize distribution of virus (Fig. 1). As GFP was originally identified from the jellyfish *Aequorea victoria*, and broadly used for molecular and functional monitoring of cellular processes, GFP is considered nontoxic to normal tissues.[11,29] We demonstrated that OBP-401 effectively destroyed a variety of human cancer cells *in vitro*, and that such effect was markedly enhanced when it was combined with docetaxel (Figs. 2 and 3). Quantitative real-time PCR analysis showed that intracellular amplification of OBP-401 and viral release into the culture supernatants were not affected by docetaxel (Fig. 4), suggesting that the latter did not alter viral replication *in vitro*. Low-dose taxanes induced G2/M arrest without inhibiting DNA synthesis, which in turn led to apoptosis, whereas OBP-401 infection had no effect on cell cycle distribution as demonstrated in flow cytometric analysis (data not shown). These results indicate that the antitumor machinery is different between docetaxel and OBP-401. Indeed, nuclear morphology of cells infected with OBP-401 was distinct from apoptosis, which is characterized by chromosome condensation and nuclear shrinkage and fragmentation (data not shown). Moreover, apoptosis in mammalian cells is mediated by a family of cysteine proteases known as caspases, which are the executioners of apoptosis and essential for the disassembly of the cell. Western blot analyses demonstrated no changes in procaspase-3 levels and no expression of cleaved form of caspase-3 in H1299 cells infected with OBP-401 (data not shown).

There is evidence that changes in the expression of microtubule-associated protein 4 (MAP4) affect the sensitivity to antimicrotubule drugs. Expression of MAP4 is transcriptionally repressed by wild-type p53. Increased expression of MAP4, which occurs when p53 is transcriptionally inactive, augments microtubule polymerization, taxanes binding and sensitivity to taxanes, which stabilizes polymerized microtubules.[30] Our preliminary experiments, however, demonstrated that OBP-401 infection did not affect the expression of MAP4 in human cancer cells (data not shown). Thus, the mechanism of combination effect of OBP-401 and docetaxel is still unclear.

Our *in vitro* data raise the possibility that docetaxel-mediated apoptosis and OBP-401-mediated oncolysis coexisted; these agents did not interfere with mutually and individually induced antitumor efficacy. In fact, the antitumor effect of the combination therapy was likely additive *in vitro*. To determine whether the interaction between the 2 drugs exhibited synergistic or additive cytotoxic effects, the data from a series of dose–response curves was examined by constructing isobolograms. Isobologram analysis indicated that the combination was less than synergistic across all dose levels tested (data not shown). In contrast, interestingly, intratumoral injection of OBP-401 combined with systemic administration of docetaxel induced a more pronounced inhibition of the growth of H1299 tumor xenografts over a long period of time (Fig. 5). Therefore, there might be some particular interactions between OBP-401 and docetaxel to produce a synergistic effect *in vivo*. It has been reported that metronomic chemotherapy, which refers to the chronic administration of comparatively low doses of cytotoxic drugs at close, regular intervals has an antiangiogenic basis.[31] Like our approach, the potent antiangiogenic capacity of drug administered in a metronomic fashion finds favor in a number of *in vivo* preclinical studies; to prove this efficacy with *in vitro* experiments is, however, technically difficult. There are some possible explanations for the superior *in vivo* antitumor activity in our experiments. Systemically administered docetaxel may attack the vascular endothelial cells in the tumor site, which in turn can block the escape of locally injected OBP-401 into the blood circulation. Another possibility is that OBP-401 itself may inhibit the vascular supply by killing endothelial cells. Virtually, the exact mechanism of this *in vivo* combination effect needs further examination.

In summary, our data demonstrated that the combination of OBP-401 and docetaxel efficiently inhibited human cancer cell growth both *in vitro* and *in vivo*, an outcome that has important implications for tumor-specific oncolytic chemovirotherapies for human cancers.

References

1. Blackburn EH. Structure and function of telomeres. Nature (Lond.) 1991;350:569–73.
2. Kim NW, Piatyszek MA, Prowse KR, Harley CB, West MD, Ho PL, Coviello GM, Wright WE, Weinrich SL, Shay JW. Specific association of human telomerase activity with immortal cells and cancer. Science 1994;266:2011–5.
3. Shay JW, Wright WE. Telomerase activity in human cancer. Curr Opin Oncol 1996;8:66–71.
4. Nakayama J, Tahara H, Tahara E, Saito M, Ito K, Nakamura H, Nakanishi T, Tahara E, Ide T, Ishikawa F. Telomerase activation by hTRT in human normal fibroblasts and hepatocellular carcinomas. Nat Genet 1998;18:65–8.
5. Bischoff JR, Kirn DH, Williams A, Heise C, Horn S, Muna M, Ng L, Nye JA, Sampson-Johannes A, Fattaey A, McCormick F. An adenovirus mutant that replicates selectively in p53-deficient human tumor cells. Science 1996;274:373–6.
6. Rodriguez R, Schuur ER, Lim HY, Henderson GA, Simons JW, Henderson DR. Prostate attenuated replication competent adenovirus (ARCA) CN706: a selective cytotoxic for prostate-specific antigen-positive prostate cancer cells. Cancer Res 1997;57:2559–63.
7. Tsukuda K, Wiewrodt R, Molnar-Kimber K, Jovanovic VP, Amin KM. An E2F-responsive replication-selective adenovirus targeted to the defective cell cycle in cancer cells: potent antitumoral efficacy but no toxicity to normal cell. Cancer Res 2002;62:3438–47.
8. Li Y, Yu DC, Chen Y, Amin P, Zhang H, Nguyen N, Henderson DR. A hepatocellular carcinoma-specific adenovirus variant, CV890, eliminates distant human liver tumors in combination with doxorubicin. Cancer Res 2001;61:6428–36.
9. Kirn D, Martuza RL, Zwiebel J. Replication-selective virotherapy for cancer: biological principles, risk management and future directions. Nat Med 2001;7:781–7.
10. Kawashima T, Kagawa S, Kobayashi N, Shirakiya Y, Umeoka T, Teraishi F, Taki M, Kyo S, Tanaka N, Fujiwara T. Telomerase-specific replication-selective virotherapy for human cancer. Clin Cancer Res 2004;10:285–92.
11. Umeoka T, Kawashima T, Kagawa S, Teraishi F, Taki M, Nishizaki M, Kyo S, Nagai K, Urata Y, Tanaka N, Fujiwara T. Visualization of intrathoracically disseminated solid tumors in mice with optical imaging by telomerase-specific amplification of a transferred green fluorescent protein gene. Cancer Res 2004;64:6259–65.
12. Taki M, Kagawa S, Nishizaki M, Mizuguchi H, Hayakawa T, Kyo S, Nagai K, Urata Y, Tanaka N, Fujiwara T. Enhanced oncolysis by a tropism-modified telomerase-specific replication-selective adenoviral agent OBP-405 ('Telomelysin-RGD'). Oncogene 2005;24:3130–40.
13. Khuri FR, Nemunaitis J, Ganly I, Arseneau J, Tannock IF, Romel L, Gore M, Ironside J, MacDougall RH, Heise C, Randlev B, Gillenwater AM, et al. A controlled trial of intratumoral ONYX-015, a selectively-replicating adenovirus, in combination with cisplatin and 5-fluorouracil in patients with recurrent head and neck cancer. Nat Med 2000;6:879–85.
14. Reid T, Galanis E, Abbruzzese J, Sze D, Wein LM, Andrews J, Randlev B, Heise C, Uprichard M, Hatfield M, Rome L, Rubin J, et al. Hepatic arterial infusion of a replication-selective oncolytic adenovirus (dl1520): phase II viral, immunologic, and clinical endpoints. Cancer Res 2002;62:6070–9.
15. Hecht JR, Bedford R, Abbruzzese JL, Lahoti S, Reid TR, Soetikno RM, Kirn DH, Freeman SM. A phase I/II trial of intratumoral endoscopic ultrasound injection of ONYX-015 with intravenous gemcitabine in unresectable pancreatic carcinoma. Clin Cancer Res 2003;9:555–61.
16. Galanis E, Okuno SH, Nascimento AG, Lewis BD, Lee RA, Oliveira AM, Sloan JA, Atherton P, Edmonson JH, Erlichman C, Randlev B, Wang Q, et al. Phase I-II trial of ONYX-015 in combination with MAP chemotherapy in patients with advanced sarcomas. Gene Ther 2005;12:437–45.

17. Dumontet C, Sikic B. Mechanisms of action of and resistance to antitubulin agents: microtubule dynamics, drug transport, and cell death. J Clin Oncol 1999;17:1061–70.
18. Jordan M, Toso R, Thrower D, Wilson L. Mechanism of mitotic block and inhibition of cell proliferation by taxol at low concentrations. Proc Natl Acad Sci USA 1993;90:9552–6.
19. Tsunemitsu Y, Kagawa S, Tokunaga N, Otani S, Umeoka T, Roth JA, Fang B, Tanaka N, Fujiwara T. Molecular therapy for peritoneal dissemination of xenotransplanted human MKN-45 gastric cancer cells with adenovirus mediated Bax gene transfer. Gut 2004;53:554–60.
20. Peters AH, Drumm J, Ferrell C, Roth DA, Roth DM, McCaman M, Novak PL, Friedman J, Engler R, Braun RE. Absence of germline infection in male mice following intraventricular injection of adenovirus. Mol Ther 2001;4:603–13.
21. Nemunaitis J, Ganly I, Khuri F, James Arseneau J, Kuhn J, McCarty T, Landers S, Maples P, Romel L, Randlev B, Reid T, Kaye S, et al. Selective replication and oncolysis in p53 mutant tumors with ONYX-015, an E1B-55kD gene-deleted adenovirus, in patients with advanced head and neck cancer: a phase II trial. Cancer Res 2000; 60:6359–66.
22. Jacobs C, Lyman G, Velez-Garcia E, Sridhar KS, Knoght W, Hochster H, Goodnough LT, Mortimer JE, Einhorn LH, Schacter LA. Phase III randomized study comparing cisplatin and fluorouracil as single agents and in combination for advanced squamous cell carcinoma of the head and neck. J Clin Oncol 1992;10:257–63.
23. Vokes EE. Chemotherapy and integrated treatment approaches in head and neck cancer. Curr Opin Oncol 1991;3:529–34.
24. Heise C, Sampson-Johannes A, Williams A, McCormick F, Von Hoff DD, Kirn DH. ONYX-015, an E1B gene-attenuated adenovirus, causes tumor-specific cytolysis and antitumoral efficacy that can be augmented by standard chemotherapeutic agents. Nat Med 1997;3: 639–45.
25. You L, Yang CT, Jablons DM. ONYX-015 works synergistically with chemotherapy in lung cancer cell lines and primary cultures freshly made from lung cancer patients. Cancer Res 2000;60:1009–13.
26. Toyoizumi T, Mick R, Abbas AE, Kang EH, Kaiser LR, Molnar-Kimber KL. Combined therapy with chemotherapeutic agents and herpes simplex virus type 1 ICP34.5 mutant (HSV-1716) in human non-small cell lung cancer. Hum Gene Ther 1999;10:3013–29.
27. Nielsen LL, Lipari P, Dell J, Gurnani M, Hajian G. Adenovirus-mediated p53 gene therapy and paclitaxel have synergistic efficacy in models of human head and neck, ovarian, prostate, and breast cancer. Clin Cancer Res 1998;4:835–46.
28. Yu DC, Chen Y, Dilley J, Li Y, Embry M, Zhang H, Nguyen N, Amin P, Oh J, Henderson DR. Antitumor synergy of CV787, a prostate cancer-specific adenovirus, and paclitaxel and docetaxel. Cancer Res 2001;61:517–25.
29. Richards HA, Han CT, Hopkins RG, Failla ML, Ward WW, Stewart CN. Safety assessment of recombinant green fluorescent protein orally administered to weaned rats. J Nutr 2003;133:1909–12.
30. Zhang CC, Yang JM, Bash-Babula J, White E, Murphy M, Levine AJ, Hait WN. DNA damage increases sensitivity to vinca alkaloids and decreases sensitivity to taxanes through p53-dependent repression of microtubule-associated protein 4. Cancer Res 1999;59:3663–70.
31. Shaked Y, Emmenegger U, Francia G, Chen L, Lee CR, Man S, Paraghamian A, Ben-David Y, Kerbel RS. Low-dose metronomic combined with intermittent bolus-dose cyclophosphamide is an effective long-term chemotherapy treatment strategy. Cancer Res 2005;65: 7045–51.

nature medicine

In vivo imaging of lymph node metastasis with telomerase-specific replication-selective adenovirus

Hiroyuki Kishimoto[1,2], Toru Kojima[1,2], Yuichi Watanabe[1,3], Shunsuke Kagawa[1,2], Toshiya Fujiwara[1,2], Futoshi Uno[1,2], Fuminori Teraishi[1,2], Satoru Kyo[4], Hiroyuki Mizuguchi[5], Yuuri Hashimoto[3], Yasuo Urata[3], Noriaki Tanaka[1] & Toshiyoshi Fujiwara[1,2]

Currently available methods for detection of tumors *in vivo* such as computed tomography and magnetic resonance imaging are not specific for tumors. Here we describe a new approach for visualizing tumors whose fluorescence can be detected using telomerase-specific replication-competent adenovirus expressing green fluorescent protein (GFP) (OBP-401). OBP-401 contains the replication cassette, in which the human telomerase reverse transcriptase (hTERT) promoter drives expression of *E1* genes, and the *GFP* gene for monitoring viral replication. When OBP-401 was intratumorally injected into HT29 tumors orthotopically implanted into the rectum in BALB/c *nu/nu* mice, para-aortic lymph node metastasis could be visualized at laparotomy under a three-chip color cooled charged-coupled device camera. Our results indicate that OBP-401 causes viral spread into the regional lymphatic area and selectively replicates in neoplastic lesions, resulting in GFP expression in metastatic lymph nodes. This technology is adaptable to detect lymph node metastasis *in vivo* as a preclinical model of surgical navigation.

Medical imaging techniques have become an essential aspect of cancer diagnosis, detection, and treatment monitoring. Advances and improvements in the major imaging modalities such as computed tomography, magnetic resonance imaging and ultrasound techniques have increased the sensitivity of visualizing tumors and their metastases in the body[1,2]. A limiting factor of these techniques is, however, the inability to specifically identify malignant tissues. Positron emission tomography with the glucose analog ^{18}F-2-deoxy-D-glucose is the first molecular imaging technique that has been widely applied for cancer imaging in clinical settings[3]. Although ^{18}F-2-deoxy-D-glucose–positron emission tomography has high detection sensitivity, it has some limitations such as the difficulty in distinguishing between proliferating tumor cells and inflammation and the inability in using it for real-time detection of tumor tissues. A relatively inexpensive, robust and straightforward way of defining the location and area of tumors *in vivo* would greatly aid the treatment of human cancer, especially for surgical procedures. In particular, if tumors too small for direct visual detection and therefore not detectable by direct inspection could be imaged *in situ*, surgeons could excise such tumors precisely with appropriate surgical margins.

Sentinel lymph node (SLN) mapping is a minimally invasive procedure and widely used in the management of patients with cutaneous melanoma or breast cancer without clinical evidence of nodal metastases[4,5]. The technique assumes that early lymphatic metastases, if present, are always found first within the SLN, the first tumor-draining lymph node. A SLN free of tumor cells would therefore predict the absence of metastatic disease in the rest of the tumor-draining lymph node basin, which indicates that intensive lymphadenectomy is unlikely to benefit those patients. Several studies have validated this assumption; the sensitivity of intraoperative frozen-section analysis for detection of nodal metastases, however, is relatively low, and high false-negative rates have been reported[6–9]. In addition, thicker primary and larger SLN tumor size has been shown to be predictive of non-SLN metastasis, presumably because of the altered lymphatic drainage routes. These findings raise doubt about the applicability of this technique in widespread surgical practice; therefore, several different approaches have been taken to directly label tumor cells to visualize and track them *in vivo*.

The GFP, which was originally identified from the jellyfish *Aequorea victoria*, is an attractive molecular marker for imaging in live tissues because of the relatively noninvasive nature of fluorescence[10–15]. We previously demonstrated a real-time fluorescence optical imaging of pleural dissemination of human non-small-cell lung cancer cells in an orthotopic mouse model using tumor-specific replication-competent adenovirus (OBP-301, Telomelysin)[16,17] in combination with replication-deficient adenovirus expressing *GFP* (Ad-*GFP*)[18]. In the present study we additionally modified OBP-301 to contain the *GFP* gene driven by the cytomegalovirus (CMV) promoter for monitoring viral replication. The resultant adenovirus, termed OBP-401, efficiently labeled tumor cells with green fluorescence *in vitro* and *in vivo*. The results showed that injection of OBP-401 into primary tumors allows its lymphatic spread, which in turn induces viral replication in

[1]Division of Surgical Oncology, Department of Surgery, Okayama University Graduate School of Medicine, Dentistry and Pharmaceutical Sciences, 2-5-1 Shikata-cho, Okayama 700-8558, Japan. [2]Center for Gene and Cell Therapy, Okayama University Hospital, 2-5-1 Shikata-cho, Okayama 700-8558, Japan. [3]Oncolys BioPharma, Inc., 3-16-33 Roppongi, Minato-ku, Tokyo 106-0032, Japan. [4]Department of Obstetrics and Gynecology, Kanazawa University School of Medicine, 13-1 Takara-machi, Kanazawa 920-8641, Japan. [5]Laboratory of Gene Transfer and Regulation, National Institute of Biomedical Innovation, 7-6-8 Saito-Asagi, Ibaraki, Osaka 567-0085, Japan. Correspondence should be addressed to T.F. (toshi_f@md.okayama-u.ac.jp).

Received 9 February; accepted 3 April; published online 1 October 2006; doi:10.1038/nm1404

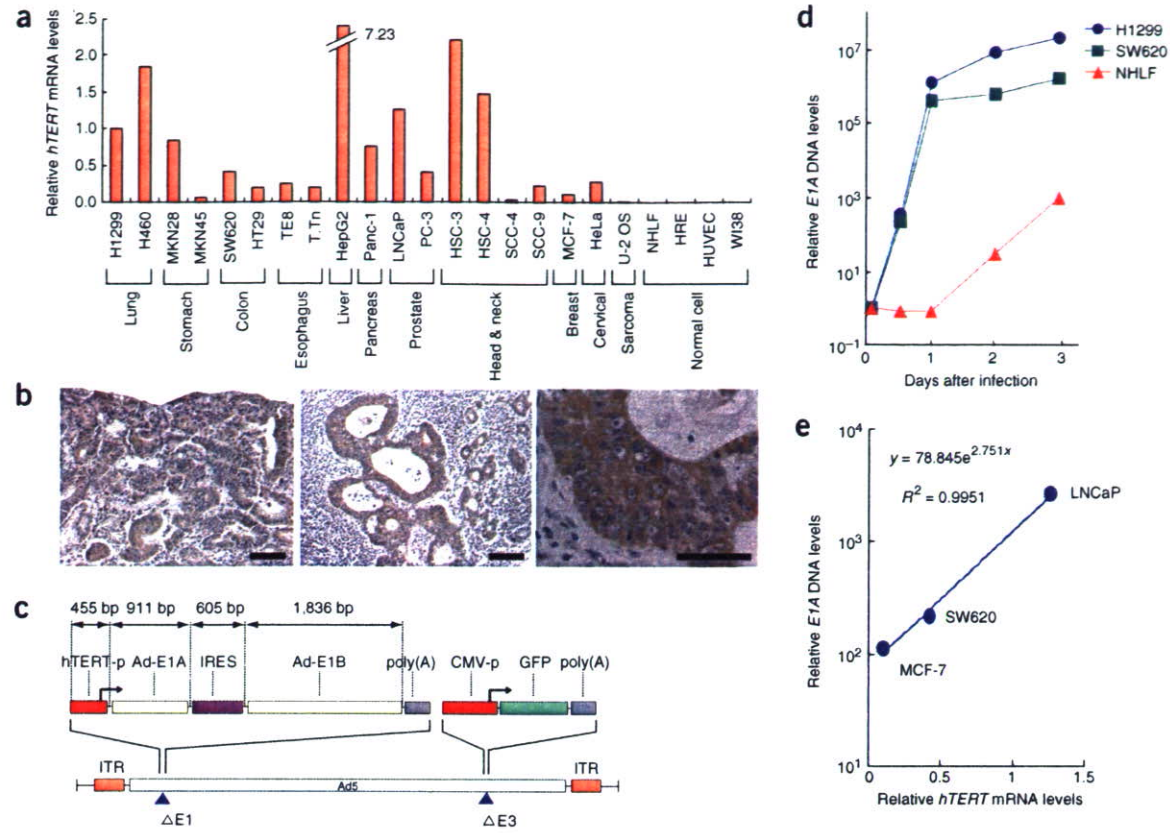

Figure 1 hTERT expression and selective replication of OBP-401 in human cancer cells. (**a**) Relative *hTERT* mRNA expression in human tumor and normal cell lines determined by real-time RT-PCR analysis. The *hTERT* mRNA expression of H1299 human lung cancer cells was considered as 1.0, and the relative expression of each cell line was calculated against that of H1299 cells. (**b**) Immunohistochemical analysis of the hTERT protein expression in surgical specimens of human gastric cancer and their microscopic metastases in lymph nodes. Representative microscopic images of primary tumor (left panel) and metastatic foci in lymph node (middle and right) are shown. Positive staining is reddish brown. Counterstain is blue-purple. Original magnification: ×200 (left and middle) and ×400 (right). Scale bar, 100 μm. (**c**) DNA structures of OBP-401. (**d**) Assessment of viral DNA replication in H1299, SW620 and NHLF cells. Cells were infected with OBP-401 at an MOI of 10 for 2 h. Subsequent to the removal of virus inocula, cells were additionally incubated for the indicated time periods and then subjected to real-time quantitative PCR assay. The amounts of viral E1A copy number are defined as the fold increases for each sample relative to that at 2 h (2 h equals 1). (**e**) Relationship between viral replication and hTERT expression determined by real-time RT-PCR analysis. Plots represent the relative *E1A* DNA levels at 24 h after OBP-401 infection and the relative *hTERT* mRNA levels in SW620, LNCaP and MCF-7 cell lines. The slope represents the positive correlation between these two factors ($R^2 = 0.9951$).

metastatic lymph nodes, thereby leading to the direct imaging of micrometastases. This technology is adaptable to detect lymph node metastasis *in vivo* as a preclinical model of surgical navigation.

RESULTS

hTERT levels in human cell lines and lymph node metastases

To confirm the specificity of telomerase activity in human cancer cells, we measured expression of *hTERT* mRNA in a panel of human tumor and normal cell lines using a real-time RT-PCR method. Although the expression varied widely, all tumor cell lines derived from different organs expressed detectable levels of *hTERT* mRNA, whereas human fibroblast cells lines such as the normal human lung fibroblast (NHLF) and normal human lung diploid fibroblast (WI38), human vascular endothelial cells, and normal human renal epithelial cells were negative for *hTERT* expression (**Fig. 1a**). We also examined samples of 30 primary tumors and 39 lymph node metastases obtained from gastric cancer patients for hTERT protein expression by immunohistochemistry (**Supplementary Table 1** online). As shown in **Fig. 1b**, hTERT staining was clearly observed in metastatic foci of gastric cancers, although most of the lymphocytes present in lymph nodes were negative for hTERT except in some germinal centers. These results suggest that the hTERT promoter element can be used to target human cancer.

Selective visualization of human cancer cells *in vitro*

We constructed the tumor-specific replication-competent adenovirus OBP-401, which expresses *GFP* by inserting the *GFP* gene under the control of the CMV promoter at the deleted E3 region of the telomerase-specific replication-selective type 5 adenovirus OBP-301 (refs. 16,17) (**Fig. 1c**). To evaluate the replication ability of OBP-401 in different cell lines, we measured the relative amounts of *E1A* DNA by quantitative real-time PCR analysis. Human cancer cells (H1299 and SW620) and normal cells (NHLFs) were infected with OBP-401 at a multiplicity of infection (MOI) of 10 for 2 h, followed by incubation in the medium. Cells were harvested at various times during the 3 d after infection, and the virus yield was determined by quantitative real-time PCR assay targeting for the viral *E1A* sequence. The ratios were normalized by dividing the value of cells obtained 2 h after viral infection. In SW620 and H1299 cells, OBP-401 replicated 6–7 logs by 3 d after infection;

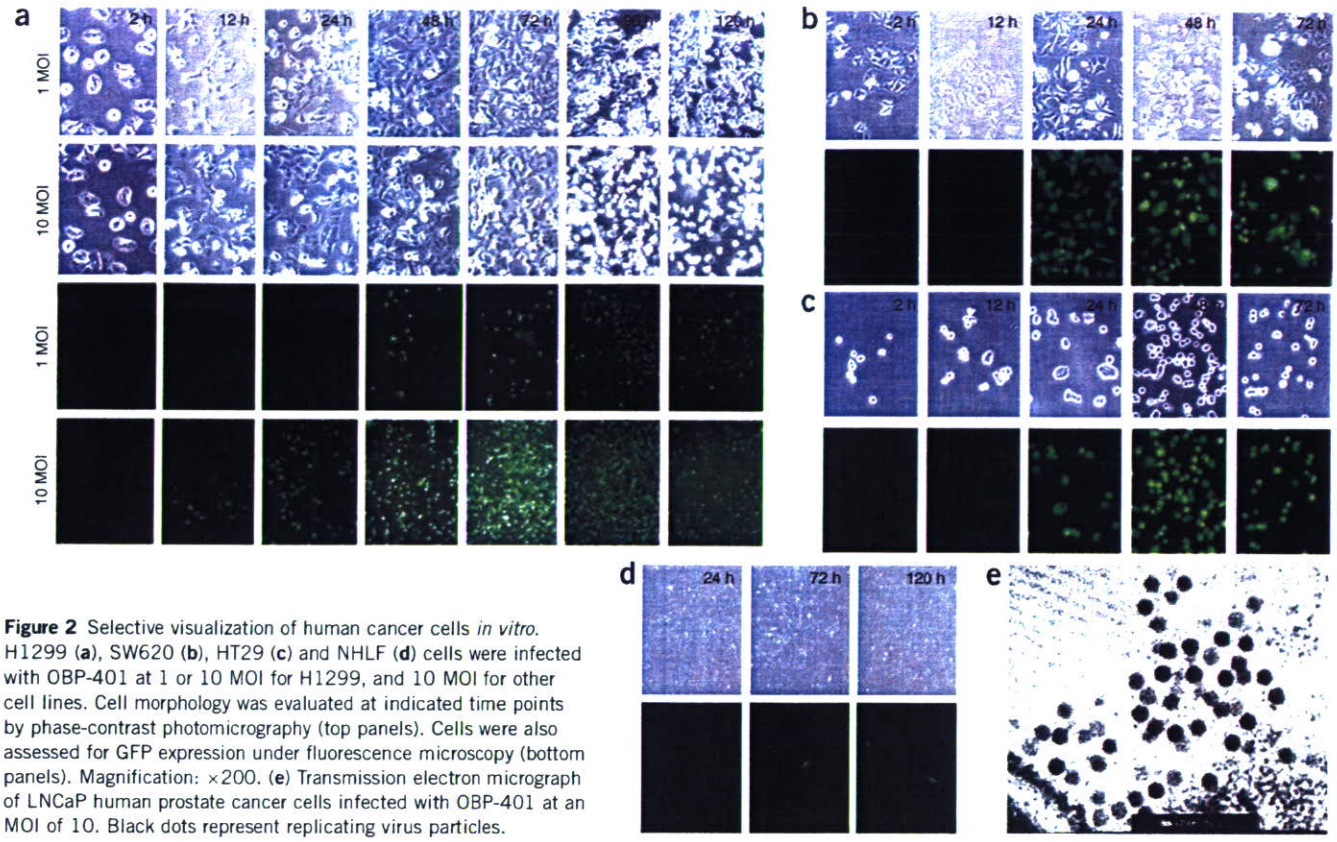

Figure 2 Selective visualization of human cancer cells *in vitro*. H1299 (**a**), SW620 (**b**), HT29 (**c**) and NHLF (**d**) cells were infected with OBP-401 at 1 or 10 MOI for H1299, and 10 MOI for other cell lines. Cell morphology was evaluated at indicated time points by phase-contrast photomicrography (top panels). Cells were also assessed for GFP expression under fluorescence microscopy (bottom panels). Magnification: ×200. (**e**) Transmission electron micrograph of LNCaP human prostate cancer cells infected with OBP-401 at an MOI of 10. Black dots represent replicating virus particles.

OBP-401 replication, however, was attenuated up to 3 logs in normal NHLFs (**Fig. 1d**). These findings indicate that OBP-401 viral recovery was reduced by 3–4 logs in normal cells as compared with cancer cells. We also found an apparent correlation between viral yields at 24 h after OBP-401 infection and *hTERT* mRNA expression in human cancer cell lines (**Fig. 1e**).

To determine whether OBP-401 replication is associated with selective GFP expression, cells were analyzed and photographed by fluorescent microscope after OBP-401 infection. As shown in **Fig. 2a**, H1299 human non-small-cell lung cancer cells expressed bright GFP fluorescence as early as 12 h after OBP-401 infection at an MOI of 10. The fluorescence intensity gradually increased in a dose-dependent fashion until ~72 h after infection, followed by rapid cell death due to the cytopathic effect of OBP-401, as shown by floating, highly light-refractile cells under phase-contrast photomicrographs. In SW620 and HT29 human colorectal cancer cells we detected GFP expression 24 h after infection with 10 MOI of OBP-401, and cells showed the cytopathic effect at 72 h after infection (**Fig. 2b,c**). In contrast, normal NHLF cells were negative for GFP expression after OBP-401 infection (**Fig. 2d**). These results indicate that OBP-401 can replicate exclusively in human cancer cells, leading to tumor cell–specific GFP fluorescence expression *in vitro*. We detected replicating virus particles in human cancer cells by transmission electron microscopy (**Fig. 2e**). The cytopathic effect of OBP-401 was also assessed by the cell viability assay using the tetrazolium salt XTT. In both SW620 and HT29 cells, OBP-401 infection induced rapid cell death in a dose-dependent manner (**Supplementary Fig. 1a** online). In *nu/nu* mice carrying subcutaneous SW620 human colorectal tumor xenografts, intratumoral injection of OBP-401 resulted in a significant inhibition of tumor growth as compared with mock-treated tumors (**Supplementary Fig. 1b** online).

Selective visualization of subcutaneous tumors *in vivo*

It is reported that the hTERT promoter could be used to induce transgene expression in syngenic tumors in mice[19]. We first confirmed that OBP-401 could replicate and express GFP fluorescence in Colon-26 cells *in vitro* as well as *in vivo* (**Supplementary Fig. 2a,b** online). In contrast, OBP-401 replication was attenuated in mouse splenocytes (**Supplementary Fig. 2a** online). These results suggest that the hTERT promoter can efficiently use the mouse transcriptional machinery and, therefore, the selectivity of OBP-401 can be examined in human tumor xenografts in mice.

To assess the specificity of the GFP-based fluorescent optical detection of tumors *in vivo*, we examined the kinetics of GFP transgene expression in subcutaneous SW620 and HT29 tumors after intratumoral injection of 1×10^7 PFU per 100 μl of OBP-401 with the charged-coupled device (CCD) noninvasive imaging system. Whole-body images of mice showed that intratumoral GFP fluorescence signals were detectable within 24 h after local delivery of viruses (**Fig. 3a**). The fluorescence intensity reached maximum levels within 4 d after injection and was maintained for at least 7 d. When SW620 tumors were removed 14 d after intratumoral injection of OBP-401, the high GFP transgene expression was visible on the surface of tumors as well as across serially sliced sections (**Fig. 3b**). No GFP fluorescence was detected when non-tumor-bearing mice were subcutaneously injected with 1×10^7 PFU per 100 μl of OBP-401 (**Fig. 3c**), suggesting confinement of GFP expression to the tumor.

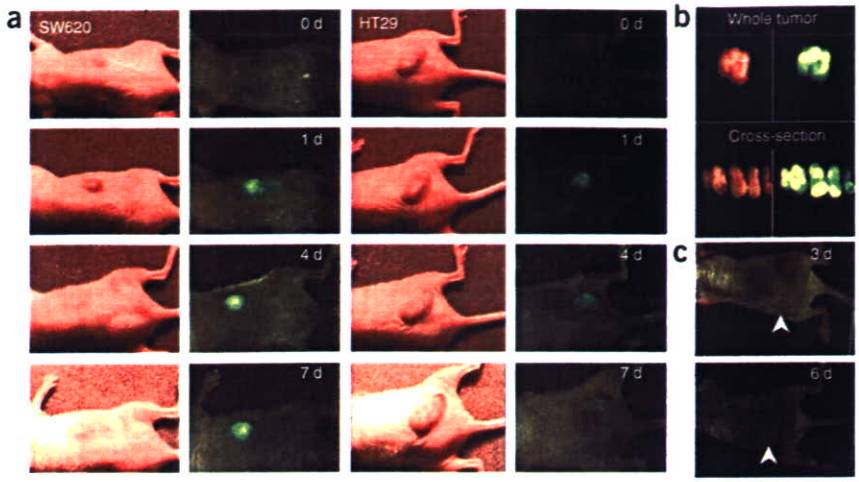

Figure 3 Selective visualization of subcutaneous tumors *in vivo*. (**a**) Time course of external images of subcutaneous SW620 and HT29 tumors after intratumoral injection of OBP-401. When tumors grew to ~6–7 mm in diameter after subcutaneous inoculation of SW620 and HT29 tumor cells (5×10^6 cells per mouse), OBP-401 viruses at the concentration of 1×10^7 PFU were directly injected into established tumors. The GFP fluorescence intensity was monitored for 7 d under the CCD noninvasive imaging system. Left panels, macroscopic appearance of subcutaneous tumors; right panels, fluorescence detection. (**b**) SW620 tumors were excised 14 d after OBP-401 injection and then assessed for GFP fluorescence as a whole tumor or in cross-sections. Left panels, macroscopic appearance of subcutaneous tumors; right panels, fluorescence detection. (**c**) Photographs of non-tumor-bearing *nu/nu* mice injected with OBP-401. Mice were subcutaneously injected with 1×10^7 PFU of OBP-401 and documented as photographs for GFP expression 3 d and 6 d after injection. Arrowheads, injected area.

Orthotopic mouse model of human rectal cancer with metastasis

The development of the orthotopic implantation technique for human rectal cancer has been described[20]. Our preliminary experiments revealed that, when 5×10^6 HT29 human colorectal cancer cells suspended in Matrigel are inoculated into the rectum submucosa of athymic *nu/nu* mice, rectal tumors appeared within 7 d after tumor injection (**Fig. 4a,b**). Histopathological examination of the excised primary tumor showed a submucosal tumor formation composed of implanted HT29 cells with a solid architecture and invasion into the muscularis propria and submucosa (**Fig. 4c**). Examination under high magnification showed tumor cell–filled lymphatic vessels in the muscularis propria layer (**Fig. 4c**). As expected, we detected the green fluorescence expression from 24 h after intratumoral administration of OBP-401 in the primary rectal tumors, with maximum signal occurring 2–4 d after injection, whereas tumors not injected with OBP-401 were completely GFP negative (**Fig. 4d**).

Selective visualization of lymph node metastasis

In our preliminary experiments, we confirmed that most mice with rectal tumors subsequently developed lymph node metastasis around the abdominal aorta from the lower margin of the renal vein to the aortic bifurcation, which were microscopically detectable ~4 weeks after tumor inoculation. Five days after injection of 1×10^8 PFU of OBP-401 into the implanted rectal tumors, we explored the abdominal cavity at laparotomy. Analyses of two representative mice are shown in **Figure 4**. Three lymph nodes (LN1, LN2 and LN3) were macroscopically identified adjacent to the aorta (**Fig. 4e,f**); the optical CCD imaging of the abdominal cavity, however, demonstrated that only one lymph node (LN3) could be detected as light-emitting spots with GFP fluorescence (**Fig. 4f**). In the other mouse, three of four lymph nodes could be imaged as GFP signals (**Fig. 4h**). We detected no GFP fluorescence in abdominal lymph nodes after injection of 1×10^7 PFU of OBP-401 into the rectal tumors (data not shown). Histopathological analysis confirmed the presence of metastatic adenocarcinoma cells in the lymph nodes with fluorescence emission, whereas GFP-negative lymph nodes contained no tumor cells (**Fig. 4g,i**). In addition, immunohistochemical analysis for GFP protein demonstrated that the reddish brown GFP-immunoreactive cells corresponded to the microscopic metastatic nodules in the lymph nodes but were not detected in the nonmetastatic lymphocyte area (**Supplementary Fig. 3** online).

We verified the GFP-based fluorescence detection with OBP-401 and histological correlation of lymph node metastasis in a series of *in vivo* experiments. Representative examples of the data are summarized in **Table 1**. Among the 7 tumor-bearing mice, 6 mice (85.7%) developed histologically confirmed lymph node metastasis. Of 28 lymph nodes excised from 7 mice, histopathological analysis demonstrated that 13 nodes (46.4%) contained micrometastatic nodules. The optical CCD imaging detected 12 lymph nodes labeled in spots with GFP fluorescence in 13 metastatic nodes (sensitivity of 92.3%). Among 15 metastasis-free lymph nodes, 2 nodes were GFP positive (specificity of 86.7%). Our results indicate that intratumoral injection of OBP-401 causes viral spread into the regional lymphatic area and selective replication in cancer cells in metastatic lymph nodes, which in turn could be imaged with GFP fluorescence. Moreover, the finding that OBP-401 did not express GFP fluorescence in a mouse para-aortic lymphadenitis model induced by inoculating complete Freund adjuvant into the rectum submucosa of

Table 1 GFP fluorescence and histopathology status in para-aortic lymph nodes of HT29 tumor-bearing mice

		GFP fluorescence[b]		
Mouse no.	Metastasis[a]	Positive	Negative	Total (%)[c]
1	Positive	1	0	1 (33.3)
	Negative	0	2	2 (66.6)
2	Positive	3	0	3 (75.0)
	Negative	0	1	1 (25.0)
3	Positive	1	0	1 (33.3)
	Negative	0	2	2 (66.6)
4	Positive	0	0	0 (0)
	Negative	0	4	4 (100)
5	Positive	1	1	2 (66.6)
	Negative	0	1	1 (33.3)
6	Positive	3	0	3 (60.0)
	Negative	1	1	2 (40.0)
7	Positive	3	0	3 (50.0)
	Negative	1	2	3 (50.0)

[a]Metastatic foci were detected histologically by hematoxylin and eosin staining. [b]Nodes with light-emitting spots and GFP fluorescence were evaluated as positive. [c]The percentage of nodes with or without histologically confirmed metastasis in each mouse.

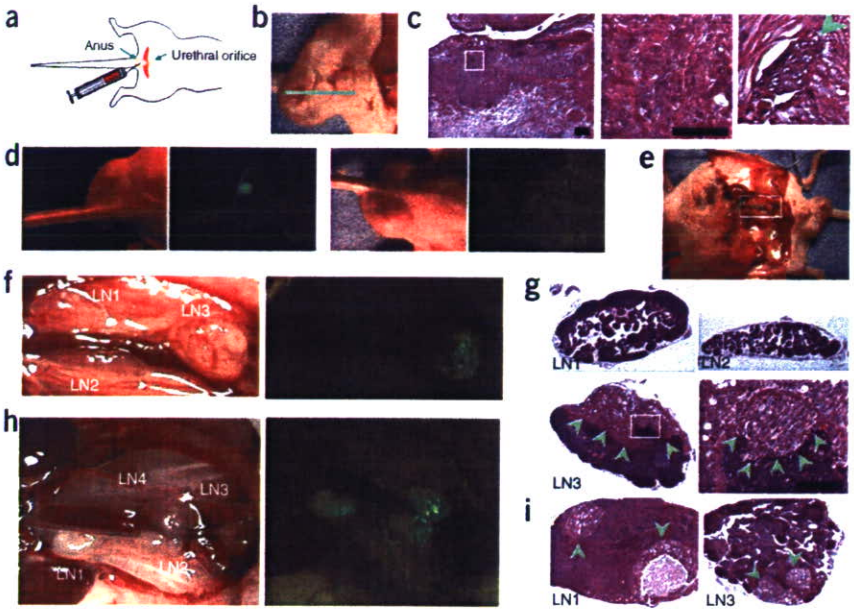

Figure 4 Orthotopic xenografts of human colorectal cancer cells and selective visualization of lymph node metastasis in two representative mice (no. 1 and no. 2). (**a**) Method used to produce HT29 human rectal tumors in BALB/c *nu/nu* mice. The rectums of mice were inoculated with 5×10^6 HT29 cells. (**b**) Macroscopic appearance of HT29 rectal tumor 4 weeks after tumor inoculation. Mice were killed and subjected to autopsy. Green line, the direction of tumor cross-sections. (**c**) Histologic sections stained with H&E showing local growth of HT29 tumor in the submucosal layer of the rectum. Scale bar, 100 μm. Left, magnification: ×40; middle (detail of the boxed region of left panel), magnification: ×400; right, lymphatic vessel invasion of HT29 tumor cells (arrowhead), magnification: ×400. (**d**) External images of orthotopic HT29 tumor-bearing *nu/nu* mice injected with OBP-401. OBP-401 at the concentration of 1×10^8 PFU were directly injected into implanted HT29 tumor (left). The GFP fluorescence could be detected as early as 24 h after OBP-401 injection under CCD imaging. Macroscopic and fluorescent images of HT29 tumor without OBP-401 injection (right). (**e**) Gross appearance of the abdominal cavity (mouse no. 1). At 5 d after intratumoral injection of OBP-401 at the concentration of 1×10^8 PFU, HT29 tumor-bearing *nu/nu* mice were assessed for lymph node metastasis at laparotomy. The white box outlines a region of **f**. (**f**) Three para-aortic lymph nodes were identified in mouse no. 1 (LN1, LN2 and LN3) (left). Internal imaging with the optical CCD camera visualized one of three nodes with GFP fluorescence (LN3) (right). (**g**) H&E staining of lymph node sections. Lymph nodes without metastatic tumors (LN1 and LN2). Lymph node containing metastatic tumors (arrowheads) (LN3) (Left, magnification: ×200; right, magnification: ×400). Scale bar, 100 μm. (**h**) Four para-aortic lymph nodes were identified in mouse no. 2 (LN1, LN2, LN3 and LN4) (left). Three of four nodes were positive for light-emitting spots with GFP fluorescence (LN1, LN2 and LN3) (right). (**i**) Histopathological detection of metastatic foci in nodes (LN1 and LN3) (arrowheads).

immunocompetent BALB/c mice suggests that this strategy could distinguish cancer metastasis from inflammatory lymphadenopathy (**Supplementary Fig. 4** online).

DISCUSSION

Lymph node status provides important information for both the diagnosis and treatment of human cancer[21,22]. Lymphatic invasion is one of the major routes for cancer cell dissemination, and adequate resection of locoregional lymph nodes is required for curative treatment in patients with advanced malignancies. The risk of having lymph node metastasis can be partially predicted by clinical data such as tumor stage, serum tumor marker concentration and medical images; there are, however, no noninvasive approaches to accurately predict the presence of lymph node metastasis, in particular, microscopic metastasis.

The specific aim of the present study was to determine the suitability of telomerase-specific amplification of the *GFP* gene for real-time imaging tumor tissues and, if so, detect nodal metastasis *in vivo* before the traditional, cumbersome procedures of histopathological examination. GFP-based fluorescence imaging can allow real-time detection of target cells without time-consuming steps such as fixation and tissue processing[13–15]. Indeed, Yang *et al.* have shown that GFP-expressing tumors growing and metastasizing in intact animals could be viewed externally with a whole-body optical imaging system[13]. Moreover, the *GFP* gene could be delivered to metastatic tumor cells *in vivo* by viral vectors[14].

To distinguish normal from neoplastic tumor tissues, selective labeling of tumor cells is required. OBP-401 produced a viral yield of 6–7 logs in human cancer cells within 3 d of infection, which was 3–4 logs higher than that in normal cells, suggesting the reliable tumor selectivity of OBP-401. Although the reason why OBP-401 replicated slightly in NHLFs despite the lack of *hTERT* mRNA expression is unclear, the fact that NHLFs could be maintained in the culture up to passages 10–20 indicates that NHLFs might have a weak telomerase activity that is undetectable by standard PCR assay. However, the attenuated replication property of OBP-401 in normal cells seems not to interfere with the visualization of tumor cells *in vivo*. In fact, we detected no GFP expression in adjacent normal tissues in subcutaneous human cancer xenografts after intratumoral injection of OBP-401, although the cross-sections of the tumor were entirely imaged with GFP fluorescence. Thus, OBP-401 provides possible probing of tumor cells *in vivo*.

Experiments using a three-CCD optical imaging system demonstrated that metastatic lymph nodes could be detected at laparotomy in mice 5 d after OBP-401 injection into implanted primary human rectal tumors. Notably, metastatic lymph nodes were imaged in spots with GFP fluorescence, which coincided with histologically confirmed micrometastasis. This experiment mimics the clinical scenario in which patients with gastrointestinal malignancies with lymph node metastasis undergo surgery, and the data suggest that the surgeon can identify metastatic lymph nodes by illuminating the abdominal cavity with a xenon lamp. The sensitivity and specificity of this imaging strategy are 92.3% and 86.7%, respectively; these results are sufficiently reliable to support the concept of this approach. In our phase I trial of a replication-deficient adenovirus vector expressing the wild-type *p53* gene (AdCMV-*p53*, ADVEXIN), DNA-PCR analysis targeting the viral genome indicated that the virus was present in tumor tissue as well as proximal lymph nodes, suggesting regional spread of the vector via the lymphatic vessels[23]. Therefore, OBP-401 is likely to be accessible to the regional lymph nodes via intratumoral administration in humans.

Currently, analysis of lymph nodes with H&E staining and microscopic examination usually involves review of only one or two tissue sections, and small foci of tumor cells can be missed. For intraoperative frozen-section analysis of SLNs, this underestimation is even more pronounced as a result of poor tissue architecture. In the treatment of breast cancer and melanoma, in which SLN biopsy is commonly used, the sensitivity of intraoperative frozen-section analysis ranges from 38% to 74% (refs. 6–9). In our experiments, additional serial sectioning was needed in 4 of 12 (33.3%) lymph nodes with GFP fluorescence to detect micrometastasis. This finding suggests that this GFP-based approach has higher sensitivity for detecting occult lymph node metastasis as compared with standard histopathological examination. Thus, the two GFP-positive nodes, in which tumor cells were not detected histologically, could have contained microscopic metastasis that would have been identified by further sectioning. Other possible explanations of false-positive detection include either that GFP protein itself was produced in the primary tumor spread into regional lymph nodes or that high doses of OBP-401 entered nodes and incidentally replicated in normal lymphocytes in that they have low telomerase activity[24].

Although the molecular imaging strategy using OBP-401 is considered promising, some limitations of the system exist, the main one being the relatively short wavelength of excitation light of GFP. In contrast to luciferase, which is also commonly used for molecular imaging[25], if objects are located in the deep layer or covered with thick adjacent tissues, the excitation light for GFP may not be able to reach them. For example, when tumor foci were exposed to the surface of nodes opposite the illuminated field, GFP fluorescence could not be detected, thereby leading to false-negative detection. The extension of exposure time to the illumination allows increasing the fluorescence intensity; the excitation light, however, cannot penetrate deeper. To raise the imaging sensitivity, one possible approach is to make the specimen thinner, for example, by pressing the excised lymph nodes flat; the architecture of the nodes, however, may be destroyed. Alternatively, it might be useful to develop a hand-held probe, in which the outlet of the excitation beam light and the sensor of GFP fluorescence are combined. During surgery, metastatic lymph nodes could be positively identified with GFP fluorescence guided by this probe like a gamma probe for SLN biopsy. At least, a hand-held flashlight to excite GFP fluorescence has been reported[26].

Administration of OBP-401 can provide an additional advantage in cancer therapy. OBP-401, similar to OBP-301, is an oncolytic virus and selectively kills human tumor cells by viral replication; the process of cell death by OBP-401, however, is relatively slow in comparison with apoptosis-inducing chemotherapeutic drugs, because the virus needs time for replication. Therefore, tumor cells infected with OBP-401 express GFP fluorescence and then lose viability, allowing the timing of detection. We could speculate that OBP-401 would spread into the regional lymph nodes after intratumoral injection, express GFP signals in tumor cells by virus replication and finally kill tumor cells even if the surgeon failed to remove all nodes containing micrometastasis. Thus, the oncolytic activity of OBP-401 may function as a backup safety antitumor program.

In conclusion, we have demonstrated that the GFP-expressing telomerase-specific replication-selective adenovirus OBP-401 can be delivered into human tumor cells in regional lymph nodes and replicate with selective GFP fluorescence after injection into the primary tumor in an orthotopic rectal tumor model. The feasibility of original OBP-301 (Telomelysin) for human cancer therapy will be confirmed in clinical trials in the near future. Because the safety profiles of these two viruses are considered homologous, this molecular imaging strategy using OBP-401 has a potential of being widely available in humans as a navigation system in the surgical treatment of malignancy.

METHODS

Cell culture. The human non-small-cell lung cancer cell lines H1299 and H460, the human gastric cancer cell lines MKN28 and MKN45, the human colorectal cancer cell lines SW620 and HT29, the human esophageal cancer cell lines TE8 and T.Tn, the human prostate cancer cell lines LNCaP and PC-3, the human tongue squamous carcinoma cell lines HSC-3, HSC-4, SCC-4 and SCC-9, the human cervical adenocarcinoma cell line HeLa, the human hepatocellular carcinoma cell line HepG2, the human pancreatic cancer cell line Panc-1, the human mammary gland adenocarcinoma cell line MCF-7, the human osteosarcoma cell line U-2OS (ATCC), the NHLF cell line, the normal human renal epithelial cell line HRE, the human umbilical vascular endothelial cell line HUVEC (TaKaRa Biomedicals) and the normal human lung diploid fibroblast cell line WI38 (HSRRB) were cultured according to the vendor's specifications.

OBP-401. OBP-401 is a telomerase-specific replication-competent adenovirus variant in which the hTERT promoter element drives the expression of *E1A* and *E1B* genes linked with an internal ribosome entry site, with the *GFP* gene inserted under the CMV promoter into the E3 region for monitoring viral replication[27,28]. The virus was purified by ultracentrifugation in cesium chloride step gradients, their titers were determined by a plaque-forming assay using 293 cells and they were stored at −80 °C.

Quantitative real-time PCR analysis. Total RNA from the cultured cells was obtained using the RNeasy Mini Kit (QIAGEN). The *hTERT* mRNA copy number was determined by real-time quantitative RT-PCR using a LightCycler instrument and a LightCycler DNA TeloTAGGG Kit (Roche Molecular Biochemicals). DNA was extracted with the QIAamp DNA Mini Kit (QIAGEN), and quantitative real-time PCR assay for the *E1A* gene was also performed. The sequences of specific primers used for *E1A* were, sense: 5′-CCTGTGTCTAGAGAATGCAA-3′; antisense: 5′-ACAGCTCAAGTCCAAAG GTT-3′. PCR amplification began with a 600-s denaturation step at 95 °C and then 40 cycles of denaturation at 95 °C for 10 s, annealing at 58 °C for 15 s and extension at 72 °C for 8 s. Data analysis was performed using LightCycler Software (Roche Molecular Biochemicals). The ratios normalized by dividing the value of untreated cells were presented for each sample.

Fluorescence microscopy. Human cancer cell lines (H1299, SW620 and HT29) and normal cells (NHLFs) were infected with either 1 or 10 MOI of OBP-401 for 2 h *in vitro*. Expression of the *GFP* gene was assessed and photographed (magnification: ×200) using an Eclipse TS-100 fluorescent microscope (Nikon).

Electron microscopy. Human prostate cancer cell line LNCaP was infected with 10 MOI of OBP-401. Thin sections were cut on coated copper grids and stained with uranyl acetate. The samples were examined and photographed with a Hitachi H-7100 transmission electron microscope.

Immunohistochemistry. Immunohistochemical staining was performed using a Histofine SAB PO kit (Nichirei) according to the manufacturer's instructions. Paired tissues of primary tumors and lymph node metastases were obtained from gastric cancer patients who underwent surgery at Okayama University Hospital. Informed consent was obtained from each individual as approved by the Ethics Review Committee for Clinical Investigation of our institution. Formalin-fixed, paraffin-embedded tissue sections were mounted on silanized slides and deparaffinized. After blocking of nonspecific reactivity with rabbit or goat serum for 10 min at 25 °C, sections were incubated overnight at 4 °C with the monoclonal antibody to hTERT (Kyowa Medex). After rinsing, the slides were incubated with biotinylated rabbit antibody to mouse, and then with avidin-biotin-peroxidase complex. Peroxidase activity was determined using DAB-H_2O_2 solution (Histofine DAB substrate kit; Nichirei). The slides were counterstained with methyl green and Mayer's hematoxylin.

Animal experiments. The experimental protocol was approved by the Ethics Review Committee for Animal Experimentation of our institution. We

produced SW620 and HT29 xenografts on the back in 5-week-old female BALB/c *nu/nu* mice by subcutaneous injection of 5×10^6 SW620 or HT29 cells in 100 µl of HBSS using a 27-gauge needle. When tumors grew to ~6–7 mm in diameter, both tumors were intratumorally injected with OBP-401 (1×10^7 PFU/100 µl). Mice were anesthetized by intraperitoneal injection of pentobarbital (50 mg/kg) and examined for GFP expression. Six mice were used for each tumor cell line. To generate an orthotopic rectal cancer model, female BALB/c *nu/nu* mice were anesthetized and then placed in a supine position. The anorectal wall was cut at a length of 7 mm to prevent colonic obstruction resulting from rectal tumor progression. We injected cell suspension of HT29 cells at a density of 5×10^6 cells in 100 µl of Matrigel basement membrane matrix (Becton Dickinson Labware) slowly into the submucosal layer of the rectum through a 27-gauge needle (**Fig. 4a**). Four weeks later we injected 1×10^8 PFU/100 µl of OBP-401 directly into the rectal tumors. Mice were killed, and their abdominal spaces were examined at laparotomy 5 d after virus injection.

Cooled CCD imaging. *In vivo* GFP fluorescence imaging was acquired by illuminating the animal with a xenon 150-W lamp. The re-emitted fluorescence was collected through a long-pass filter on a Hamamatsu C5810 3-chip color CCD camera (Hamamatsu Photonics Systems). High-resolution images were acquired using an EPSON PC. Images were processed for contrast and brightness with the use of Adobe Photoshop 4.0.1J software (Adobe).

Note: Supplementary information is available on the Nature Medicine website.

ACKNOWLEDGMENTS

This work was supported in part by grants from the Ministry of Education, Culture, Sports, Science, and Technology of Japan (T.F. and S.K.); and by grants from the Ministry of Health, Labour, and Welfare of Japan (T.F.). We thank K. Nagai and H. Kawamura for the helpful discussion, and Y. Shirakiya and N. Mukai for the excellent technical support.

AUTHOR CONTRIBUTIONS

T.F. conceived the idea for this project, designed all experiments and wrote the manuscript. H.K., Y.W. and Y.H. performed all laboratory experiments and H.K., T.K. and Y.W. performed all animal experiments. S.K. provided crucial ideas and helped with data interpretation. T.F., F.U., F.T. and N.T. provided technical assistance. S.K. provided the hTERT promoter. H.M. constructed the OBP-401 virus. Y.U. developed a protocol for virus manufacture and validation.

COMPETING INTERESTS STATEMENT

The authors declare competing financial interests (see the *Nature Medicine* website for details).

Published online at http://www.nature.com/naturemedicine/
Reprints and permissions information is available online at http://npg.nature.com/reprintsandpermissions/

1. Tearney, G.J. *et al. In vivo* endoscopic optical biopsy with optical coherence tomography. *Science* **276**, 2037–2039 (1997).
2. MacDonald, S.L. & Hansell, D.M. Staging of non-small cell lung cancer: imaging of intrathoracic disease. *Eur. J. Radiol.* **45**, 18–30 (2003).
3. Kelloff, G.J. *et al.* Progress and promise of FDG-PET imaging for cancer patient management and oncologic drug development. *Clin. Cancer Res.* **11**, 2785–2808 (2005).
4. McMasters, K.M. *et al.* Sentinel lymph node biopsy for melanoma: controversy despite widespread agreement. *J. Clin. Oncol.* **19**, 2851–2855 (2001).
5. Kuerer, H.M. & Newman, L.A. Lymphatic mapping and sentinel lymph node biopsy for breast cancer: developments and resolving controversies. *J. Clin. Oncol.* **23**, 1698–1705 (2005).
6. Koopal, S.A. *et al.* Frozen section analysis of sentinel lymph nodes in melanoma patients. *Cancer* **89**, 1720–1725 (2000).
7. Tanis, P.J. *et al.* Frozen section investigation of the sentinel node in malignant melanoma and breast cancer. *Ann. Surg. Oncol.* **8**, 222–226 (2001).
8. Gulec, S.A., Su, J., O'Leary, J.P. & Stolier, A. Clinical utility of frozen section in sentinel node biopsy in breast cancer. *Am. Surg.* **67**, 529–532 (2001).
9. Chao, C. *et al.* Utility of intraoperative frozen section analysis of sentinel lymph nodes in breast cancer. *Am. J. Surg.* **182**, 609–615 (2001).
10. Misteli, T. & Spector, D.L. Applications of the green fluorescent protein in cell biology and biotechnology. *Nat. Biotechnol.* **15**, 961–964 (1997).
11. van Roessel, P. & Brand, A.H. Imaging into the future: visualizing gene expression and protein interactions with fluorescent proteins. *Nat. Cell Biol.* **4**, E15–E20 (2002).
12. Ehrhardt, D. GFP technology for live cell imaging. *Curr. Opin. Plant Biol.* **6**, 622–628 (2003).
13. Yang, M., Baranov, E., Moossa, A.R., Penman, S. & Hoffman, R.M. Visualizing gene expression by whole-body fluorescence imaging. *Proc. Natl Acad. Sci. USA* **97**, 12278–12282 (2000).
14. Hasegawa, S. *et al. In vivo* tumor delivery of the green fluorescent protein gene to report future occurrence of metastasis. *Cancer Gene Ther.* **7**, 1336–1340 (2000).
15. Ohtani, S. *et al.* Quantitative analysis of p53-targeted gene expression and visualization of p53 transcriptional activity following intratumoral administration of adenoviral p53 *in vivo*. *Mol. Cancer Ther.* **3**, 93–100 (2004).
16. Kawashima, T. *et al.* Telomerase-specific replication-selective virotherapy for human cancer. *Clin. Cancer Res.* **10**, 285–292 (2004).
17. Taki, M. *et al.* Enhanced oncolysis by a tropism-modified telomerase-specific replication selective adenoviral agent OBP-405 ("Telomelysin-RGD"). *Oncogene* **24**, 3130–3140 (2005).
18. Umeoka, T. *et al.* Visualization of intrathoracically disseminated solid tumors in mice with optical imaging by telomerase-specific amplification of transferred green fluorescent protein gene. *Cancer Res.* **64**, 6259–6265 (2004).
19. Gu, J., Andreeff, M., Roth, J.A. & Fang, B. hTERT promoter induces tumor-specific Bax gene expression and cell killing in syngenic mouse tumor model and prevents systemic toxicity. *Gene Ther.* **9**, 30–37 (2002).
20. Tsutsumi, S., Kuwano, H., Morinaga, N., Shimura, T. & Asao, T. Animal model of paraaortic lymph node metastasis. *Cancer Lett.* **169**, 77–85 (2001).
21. Maehara, Y. *et al.* Clinical significance of occult micrometastasis in lymph nodes from patients with early gastric cancer who died of recurrence. *Surgery* **119**, 397–402 (1996).
22. Coello, M.C., Luketich, J.D., Litle, V.R. & Godfrey, T.E. Prognostic significance of micrometastasis in non-small-cell lung cancer. *Clin. Lung Cancer* **5**, 214–225 (2004).
23. Fujiwara, T. *et al.* Multicenter phase I study of repeated intratumoral delivery of adenoviral p53 (ADVEXIN) in patients with advanced non-small cell lung cancer. *J. Clin. Oncol.* **24**, 1689–1699 (2006).
24. Hiyama, K. *et al.* Activation of telomerase in human lymphocytes and hematopoietic progenitor cells. *J. Immunol.* **155**, 3711–3715 (1995).
25. Adams, J.Y. *et al.* Visualization of advanced human prostate cancer lesions in living mice by a targeted gene transfer vector and optical imaging. *Nat. Med.* **8**, 891–897 (2002).
26. Yang, M., Luiken, G., Baranov, E. & Hoffman, R.M. Facile whole-body imaging of internal fluorescent tumors in mice with an LED flashlight. *Biotechniques* **39**, 170–172 (2005).
27. Watanabe, T. *et al.* Histone deacetylase inhibitor FR901228 enhances the antitumor effect of telomerase-specific replication-selective adenoviral agent OBP-301 in human lung cancer cells. *Exp. Cell Res.* **312**, 256–265 (2006).
28. Fujiwara, T. *et al.* Enhanced antitumor efficacy of telomerase-selective oncolytic adenoviral agent OBP-401 with docetaxel: preclinical evaluation of chemovirotherapy. *Int. J. Cancer* **119**, 432–440 (2006).

Telomerase-Specific Oncolytic Virotherapy for Human Cancer with the hTERT Promoter

Toshiyoshi Fujiwara[1,2,*], Yasuo Urata[3] and Noriaki Tanaka[2]

[1]*Center for Gene and Cell Therapy, Okayama University Hospital, Okayama 700-8558, Japan;* [2]*Division of Surgical Oncology, Department of Surgery, Okayama University Graduate School of Medicine, Dentistry and Pharmaceutical Sciences, Okayama 700-8558, Japan;* [3]*Oncolys BioPharma, Inc., Tokyo 106-0032, Japan*

Abstract: Replication-selective tumor-specific viruses present a novel approach for treatment of neoplastic disease. These vectors are designed to induce virus-mediated lysis of tumor cells after selective viral propagation within the tumor. For targeting cancer cells, there is a need for tissue- or cell-specific promoters that can express in diverse tumor types and are silent in normal cells. Recent advances in molecular biology have fostered remarkable insights into the molecular basis of neoplasm. Telomerase activation is considered to be a critical step in carcinogenesis and its activity correlates closely with human telomerase reverse transcriptase (hTERT) expression. Since only tumor cells that express telomerase activity would activate this promoter, the hTERT proximal promoter allows for preferential expression of viral genes in tumor cells, leading to selective viral replication. We constructed an attenuated adenovirus 5 vector (Telomelysin, OBP-301), in which the hTERT promoter element drives expression of E1A and E1B genes linked with an internal ribosome entry site (IRES). Telomelysin replicated efficiently and induced marked cell killing in a panel of human cancer cell lines, whereas replication as well as cytotoxicity was highly attenuated in normal human cells lacking telomerase activity. Thus, the hTERT promoter confers competence for selective replication of Telomelysin in human cancer cells, an outcome that has important implications for the treatment of human cancers. This article reviews recent findings in this rapidly evolving field: cancer therapeutic and cancer diagnostic approaches using the hTERT promoter.

Keywords: Telomerase, hTERT, adenovirus, GFP, imaging.

INTRODUCTION

Human chromosomal end structures, named telomeres, serve as protective caps and consist of short tandemly repeated TTAGGG sequence [1, 2]. Telomere attrition contributes to genomic instability and may thereby promote the development of malignant cell transformation [3]. A fundamental difference in the behavior of normal versus tumor cells is that normal cells divide for a limited number of times, while tumor cells have the ability to proliferate indefinitely [4-6]. Telomere shortening sets a physical limit to the potential number of cell divisions and serves as a mitotic clock defining the lifespan of somatic cells [7]. One mechanism to escape this limitation is the activation or upregulation of telomerase. As telomerase can reset the mitotic clock, it has been linked to the processes of tumorigenesis and aging. Telomerase is a ribonucleoprotein complex responsible for adding TTAGGG repeats onto the 3' ends of chromosomes [8-10]. Many studies have demonstrated that the majority of malignant tumors express telomerase activity, a feature that accounts for their proliferative capacity [11-13], whereas telomerase is strongly repressed in most normal somatic tissues [14]. Therefore, telomerase has attracted considerable attention as a plausible target for cancer diagnosis and therapy [15].

The human telomerase complex is composed of three components: the RNA subunit (known as hTR, hTER, or hTERC) [16], the telomerase-associated protein (hTEP1) [17], and the catalytic subunit (hTERT, human telomerase reverse transcriptase) [18, 19]. Both hTR and hTERT are required for the reconstitution of telomerase activity *in vitro* [20] and, therefore, represent the minimal catalytic core of telomerase in humans [21]. However, while hTR is widely expressed in embryonic and somatic tissue, hTERT is tightly regulated and is not detectable in most somatic cells. The cloning of the promoter region of hTERT in 1999 [22-25] facilitated the development of targeted cancer gene therapy approaches that can specifically and markedly augment transgene expression in tumor with its specificity. Telomerase-specific expression of cytotoxic or proapoptotic genes such as the diphtheria toxin A-chain, FADD, caspases, Bax, and PUMA by the hTERT promoter has been successfully achieved and reported in various gene transfer systems (e.g., plasmid and adenovirus) [26-31]. Although adenovirus-mediated Bax gene expression via the hTERT promoter elicits a therapeutic effect on tumor cells and could prevent the toxic effects on normal cells [30], the viral spread might be less than ideal after intratumoral administration.

Replication-defective, E1-deleted adenoviral vectors facilitate the efficient delivery of a variety of transgenes to target tissues and have demonstrated clear therapeutic benefits and safety in a variety of clinical studies [32-34]; a significant obstacle, however, is the limited distribution of the vectors within the tumor mass even after direct intratumoral administration. To confer specificity of infection and increase viral spread to neighboring tumor cells, the notion of using replication-competent adenoviruses has become a reality [35-37]. The fact that activation of hTERT gene expression is one of the key events during tumorigenesis [38, 39] enables the hTERT promoter to take place in the tumor-specific transcriptional control of genes essential for viral replication. We hypothesized that an adenovirus containing the hTERT promoter-driven E1 genes could be used to target a variety of tumor cells and kill them efficiently by viral replication. Moreover, this virus can be useful for cancer diagnostics, especially for detection of minute metastases *in vivo*, since more than 85% of human cancers display telomerase activity [12].

*Address correspondence to this author at the Center for Gene and Cell Therapy, Okayama University Hospital, 2-5-1 Shikata-cho, Okayama 700-8558, Japan; Tel: 81-86-235-7997; Fax: 81-86-235-7884; E-mail: toshi_f@md.okayama-u.ac.jp

1568-0096/07 $50.00+.00

TELOMERASE AND CANCER

Telomerase Activation in Human Cancer

Cancer is characterized by unregulated proliferation of a certain cell population, which eventually affects normal cellular function in the human body [4-6]. To selectively target cancer cells, it is essential to identify the crucial molecular determinants involved in tumor progression. Cellular immortality is a critical step in tumorigenesis and, therefore, the molecular mechanism of the unlimited replicative capacity of tumor cells may provide universal and effective means for treating human cancer [15].

Telomeres are situated at the ends of linear chromosomes and protect them from degradation and end-to-end fusions [2]. Tumor cells can maintain telomere length predominantly due to the enzyme telomerase [8-10]. Telomerase activity is detected in about 85% of malignant tumors [12], whereas in most normal somatic tissues telomerase is absent [14]. Although weak telomerase activity is detected in peripheral blood leukocytes and in certain stem cell population [40, 41], the majority of malignant tumors express high levels of telomerase activity [11-13]. There is also a gradient increase in telomerase activity between early and late stage tumors. The strong association between telomerase activity and malignant tissue suggests that telomerase can be an essential target for the diagnosis and treatment of cancer.

The transcriptional upregulation of hTERT, a catalytic subunit of telomerase, represents the rate-limiting step in telomerase expression [18, 19], although other pathways involved in the control telomerase activity such as differential splicing of the hTERT transcript and posttranscriptional modification of the hTERT protein may exist [42]. Thus, the hTERT promoter region can be used as a fine-tuning molecular switch that works exclusively in tumor cells.

Regulation of hTERT Transcription

Recent studies have provided mechanistic insight into how the hTERT promoter can be stimulated or suppressed by oncogenic activation as well as inactivation of tumor suppressors. Various laboratories have identified transcription factors that are involved in upregulation or downregulation of hTERT transcriptional activity (Fig. 1). These reports proposed a variety of potential mechanisms of the transcriptional control of hTERT, which may help us design telomerase- or hTERT-based cancer therapies.

The hTERT promoter contains two E-boxes (CACGTG) that are binding sites for the Myc/Max/Mad network of transcriptional factors [22, 24, 43, 44]. The oncoprotein c-Myc forms a complex with the Max protein that binds as a heterodimer to activate hTERT transcription. In contrast, heterodimers with Mad1 and Max proteins result in repression of hTERT expression [45, 46]. The relative levels of c-Myc and Mad1 correlate directly with activation and repression of hTERT expression. The transcriptional factor Sp1 has been reported to cooperate with c-Myc to induce the hTERT promoter, depending on cell type, suggesting a reliance on Sp1 for full activity of c-Myc [47]. Other transcriptional factors such as ETS proteins and viral proteins also contribute to hTERT upregulation. Since epidermal growth factor (EGF) receptor and its homolog, the HER2/Neu proto-oncoprotein, stimulate phosphorylation of MAP kinases [48], which in turn activate ETS1/ETS2 [49], stimulation by EGF can lead to hTERT upregulation. The human papilloma virus (HPV) type 16 E6 protein can also associate with c-Myc and thereby activate the hTERT promoter [50-52].

In addition to Mad1, several dominant repressors that mediate hTERT downregulation have been identified. For example, the Wilm's tumor suppressor 1 (WT1) and myeloid-specific zinc finger protein 2 (MZF-2) interact with the hTERT promoter, to suppress hTERT transcription [53, 54]. Based on the preferential expression of WT1 in kidney, gonads, and spleen and of that of MZF-2 in myeloid cells, WT1 and MZF-2-mediated repression of hTERT seems tissue-specific. Other transcriptional factors, E2F-1, E2F-2, and E2F-3, also repress hTERT transcription by binding to the hTERT promoter [55, 56].

The hTERT transcription is also regulated by nuclear hormones as well as drugs that involve gene expression. Estrogen induces an increase in hTERT mRNA levels through the estrogen receptor (ER), which interacts with two estrogen response elements (EREs) in the hTERT promoter [57, 58]. Progesterone and androgen also stimulate telomerase activity through hTERT expression, although this response is likely to be indirect [59]. Furthermore, histone deacetylase (HDAC) inhibitors activate the transcription of certain genes by altering the acetylation status of nucleosomal histones. It has been reported that treatment with HDAC inhibitor, tricostatin A (TSA), could induce significant activation of hTERT mRNA

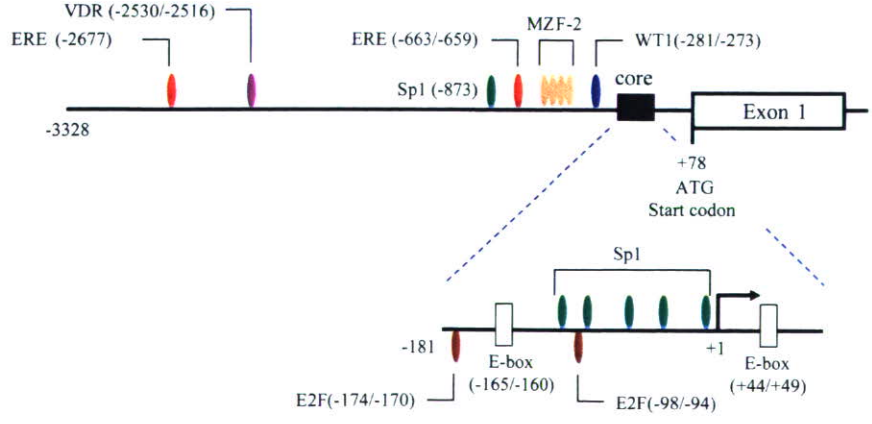

Fig. (1). Scheme of the proximal promoter of hTERT. Putative protein binding sites for various transcription factors are indicated.

expression and telomerase activity in normal cells through the TSA-responsive element localized in the hTERT proximal promoter [60]. In contrast, nonsteroidal anti-inflammatory drugs (NSAIDs) such as aspirin, indomethacin, and cyclooxygenase (COX)-2 inhibitor have been recently shown to inhibit telomerase activity at the hTERT transcriptional level in colon cancer cells [61]. The *cis*-response elements to NSAIDs have been identified in the hTERT promoter region. Furthermore, some nuclear hormone receptors including vitamin D receptor and retinoic acid receptor can repress hTERT expression [62, 63].

These observations gained from the study of hTERT transcriptional regulation suggest that hTERT activity in cancer cells can be modified by exogenous stimuli such as hormones, drugs, and genes, which may enhance the anti-tumor effects of hTERT-specific cancer therapies as combined modalities.

hTERT PROMOTER FOR CANCER THERAPEUTICS

Construction of Telomelysin

The use of modified adenoviruses that replicate and complete their lytic cycle preferentially in cancer cells is a promising strategy for treatment of cancer. One approach to achieve tumor specificity of viral replication is based on the transcriptional control of genes that are critical for virus replication such as E1A or E4. For example, the heterologous promoters from the prostate-specific antigen (PSA) [64], MUC1 [65], osteocalcin [66], L-plastin [67], midkine [68], and E2F-1 [69] genes have been used to drive E1A expression. These vectors replicate preferentially in tumor cells that express each targeted tumor marker; their therapeutic window, however, is relatively narrow because only part of the tumor is positive for each tumor marker. As described above, telomerase, especially its catalytic subunit hTERT, is expressed in the majority of human cancers and the hTERT promoter is preferentially activated in human cancer cells [12]. Thus, the broadly applicable hTERT promoter might be a suitable regulator of adenoviral replication. Indeed, it has been reported previously that the transcriptional control of E1A expression via the hTERT promoter could restrict adenoviral replication to telomerase-positive tumor cells and efficiently lyse tumor cells [70-72].

The adenovirus E1B gene is expressed early in viral infection and its gene product inhibits E1A-induced p53-dependent apoptosis, which in turn promote the cytoplasmic accumulation of late viral mRNA, leading to a shut down of host cell protein synthesis. In most vectors that replicate under the transcriptional control of the E1A gene including hTERT-specific oncolytic adenoviruses, the E1B gene is driven by the endogenous adenovirus E1B promoter. However, Li *et al.* have demonstrated that transcriptional control of both E1A and E1B genes by the α- fetoprotein (AFP) promoter with the use of IRES significantly improved the specificity and the therapeutic index in hepatocellular carcinoma cells [73]. Therefore, we have developed Telomelysin (OBP-301), in which the tumor-specific hTERT promoter regulates both the E1A and E1B genes (Fig. 2). Telomelysin controls the viral replication more stringently, thereby providing profound therapeutic effects in tumor cells as well as the attenuated toxicity in normal tissues [74].

The construction of Telomelysin was carried out as follows. An 897-bp fragment of the E1A gene and a 1822-bp fragment of the E1B gene were amplified by PCR from cellular RNA and genomic DNA of 293 cells, respectively. The amplified products were subcloned into the pTA plasmid. Following confirmation by DNA nucleotide sequencing, the E1A (911 bp) and E1B (1836 bp) genes were cloned into the pIRES vector (pE1A-IRES-E1B). A 455-bp fragment of the hTERT promoter, which contains a 378-bp region upstream of the transcription start site, was ligated into the pE1A-IRES-E1B (phTERT-E1A-IRES-E1B). The 3828-bp fragment was digested from the phTERT-E1A-IRES-E1B and then cloned into pShuttle after deletion of the cytomegalovirus (CMV) promoter. The resultant shuttle vector was applied to the Adeno-X Expression System (Clontech Laboratories, Palo Alto, CA). Recombinant adenovirus was isolated from a single plaque and expanded in 293A cells. The resultant virus was termed Telomelysin.

The 181-bp fragment upstream of the transcription start site is considered the core functional promoter that is essential for transcriptional activation of hTERT in tumor cells. Takakura *et al.* reported by analysis of 5'-truncations of the promoter that hTERT transcriptional activity decreased with deletion of sequences between -776 and -1375 and increased with the deletion of sequences between -378 and -776, indicating that *cis*-acting and silencer elements, respectively, exist in these regions [22]. They also demonstrated that the 378-bp fragment that we used for Telomelysin could exhibit high transcriptional activity similar to that of the 181-bp core promoter region.

Functional Analysis of Telomelysin

Methods used for measuring viral replication of Telomelysin include standard plaque assay using 293 cells as well as quantitative real-time PCR analysis targeting for the viral E1A or IRES sequence [74, 75], both of which present similar replication patterns of Telomelysin in human cancer cells. Telomelysin induced selective E1A and E1B expression in cancer cells, which resulted in viral replication at 5-6 logs by 3 days after infection; Telomelysin replication, however, was attenuated up to 2 logs in cultured normal cells [74, 75]. Although the transduction efficiency of adenovirus is less efficient in normal cells compared with tumor cells, the observation that wild-type adenovirus infection killed normal cultured cells more effectively suggests that the attenuated cytotoxicity of Telomelysin in normal cells is due to tumor-specific replication, but not due to the low transduction. These data indicate that selective replication of Telomelysin is both therapeutically beneficial and safe. The relative E1A DNA levels determined by quantitative real-time PCR assay after Telomelysin infection correlated with hTERT mRNA expression levels in several human cancer cell lines, suggesting that Telomelysin viral yields are closely associated with the hTERT transcriptional activity in human cancer.

The majority of human cancer cells acquire immortality and unregulated proliferation by expression of the hTERT [12] and, therefore theoretically, hTERT-specific Telomelysin can possess a broad-spectrum antineoplastic activity against a variety of human tumors. *In vitro* cytotoxicity assays demonstrated that Telomelysin could efficiently kill various types of human cancer cell lines including head and neck cancer, lung cancer, esophageal cancer, gastric cancer, colorectal cancer, breast cancer, pancreatic cancer, hepatic cancer, prostate cancer, cervical cancer, melanoma, sarcoma, and mesothelioma in a dose-dependent manner. The dose of Telomelysin that causes

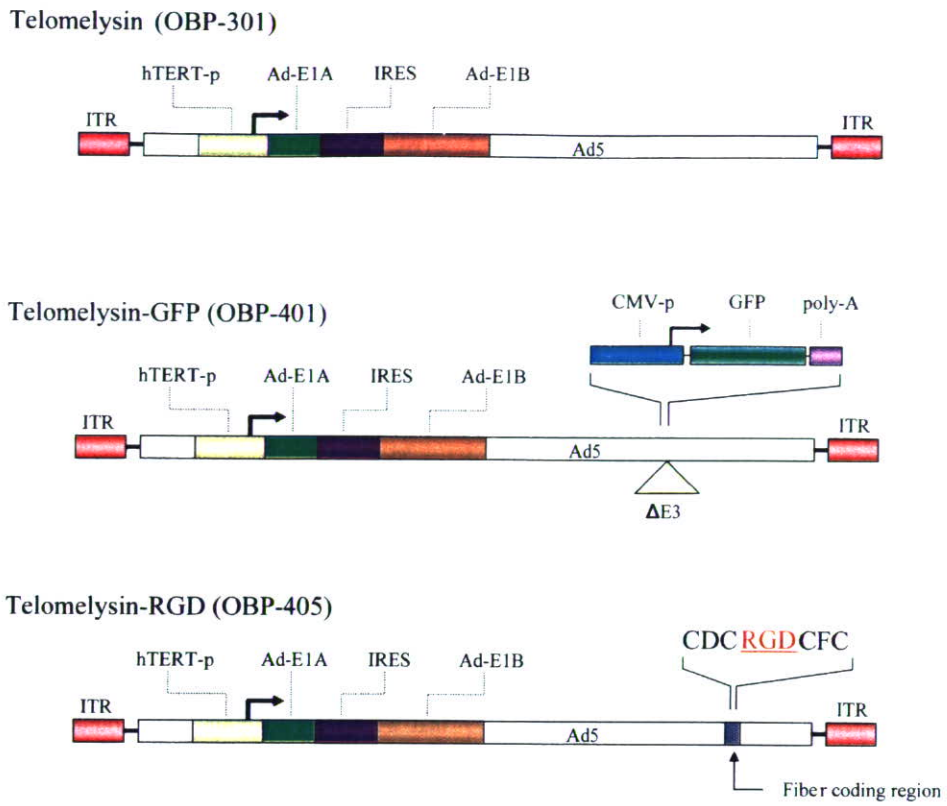

Fig. (2). Schematic DNA structures of telomerase-specific oncolytic viruses. Telomelysin (OBP-301), in which the hTERT promoter element drives the expression of E1A and E1B genes linked with an IRES. Telomelysin-GFP (OBP-401) is a telomerase-specific replication-competent adenovirus variant, in which GFP gene is inserted under CMV promoter into E3 region for monitoring viral replication. Telomelysin-RGD (OBP-405) has mutant fiber containing the RGD peptide, CDCRGDCFC, in the HI loop of the fiber knob.

about 50% reduction in cell viability in monolayer cultures (defined as ID_{50}) was less than 20 multiplicity of infections (MOIs) in almost all tumor cell lines examined in our study. These data clearly demonstrate that Telomelysin exhibits desirable features for use as an oncolytic therapeutic agent, as the proportion of cancers potentially treatable by Telomelysin is extremely high.

The *in vivo* antitumor effect of Telomelysin was also investigated by using athymic mice carrying xenografts. Intratumoral injection of Telomelysin into human tumor xenografts resulted in a significant inhibition of tumor growth and enhancement of survival [74, 75]. Macro-scopically, massive ulceration was noted on the tumor surface after injection of high-dose Telomelysin, indicating that Telomelysin induced intratumoral necrosis of tumor cells due to direct lysis by virus replication *in vivo* (Fig. **3**). For effective treatment of distant metastatic tumors, intravenously infused chemotherapeutic drugs will need to distribute in sufficient quantities into the the tumor sites; oncolytic viruses, however, could still replicate in the tumor, cause oncolysis, and then release virus particles that could reach the distant metastatic lesions. Therefore, intratumoral administration that causes the release of newly formed virus from infected tumor cells might be theoretically suitable for oncolytic virus rather than systemic administration. Indeed, it was confirmed that, following intratumoral injection, Telomelysin replicated within tumors, spread into the bloodstream, and then replicated in distant tumor sites [74, 75]. The biodistribution of Telomelysin as assessed by PCR amplification targeting for the viral E1A provides evidence that viral replication is highly specific for tumors despite its presence in the circulation. No significant elevation of liver enzymes was observed in mice intratumorally injected with Telomelysin. In addition, histopathological analysis of liver sections demonstrated absence of apoptotic hepatocytes and other histological signs of hepatocellular damage [75].

Chemotherapeutic drugs kill tumor cells mainly by inducing apoptosis, which is characterized by chromosome condensation and nuclear shrinkage and fragmentation; nuclear morphology of cells infected with Telomelysin, however, was distinct from apoptosis. Apoptosis in mammalian cells is mediated by a family of cysteine proteases known as caspases, which are the executioners of apoptosis and essential for the disassembly of the cell. No changes in procaspase-3 levels and no expression of cleaved form of caspase-3 in cells infected with Telomelysin were noted. Moreover, flow cytometric analysis demonstrated that Telomelysin infection had no effect on cell cycle distribution [76, 77]. Recently, Ito *et al.* have reported that hTERT-specific oncolytic adenovirus causes autophagic cell death, which is a type of programmed cell death that is an alternative to apoptosis, in malignant glioma cells via inhibition of the mTOR signal [78]. Although their data clearly indicate that autophagy may be one of the cell death machinery induced by oncolytic adenoviruses, our preliminary studies using the green fluorescent protein (GFP) and microtubule-associated protein 1 light chain 3 (LC3) fusion plasmid (GFP-LC3) [79] demonstrated that Telomelysin did not induce GFP-LC3 dots, which represent pre-autophagosomes and

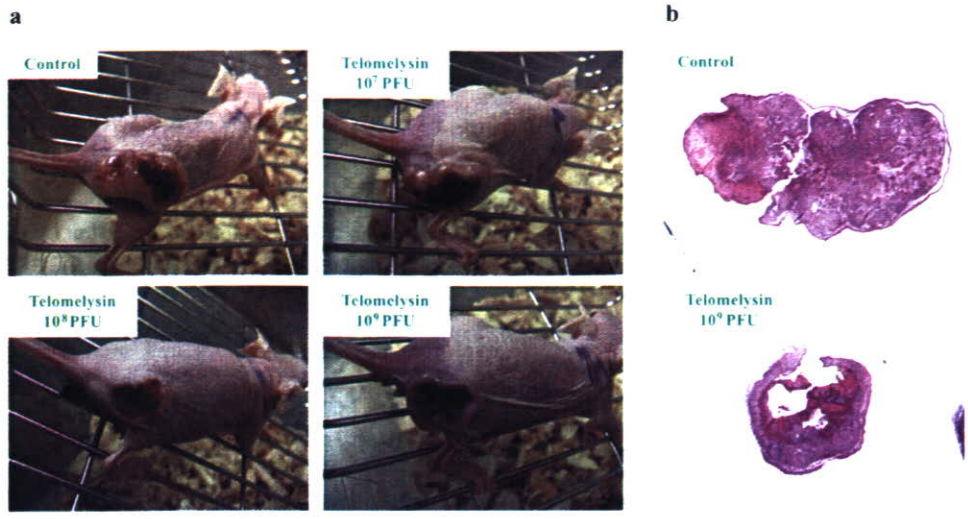

Fig. (3). Antitumor effect of intratumorally injected Telomelysin against established flank SW620 xenograft tumors in *nu/nu* mice. **(a)** Macroscopic appearance of tumors 15 days after treatment with various concentrations of Telomelysin. **(b)** Tumors were dissected 15 days after viral injection and paraffin sections were stained with hematoxylin and eosin. Massive tumor cell death at the central portions of the tumors where Telomelysin was injected was observed.

autophagosomes in human lung cancer cells. Thus, further investigation in other types of cancer cells will be required to determine the exact mechanisms of Telomelysin-triggered cell death.

Multi-Disciplinary Therapy with Telomelysin

The development of Telomelysin as a monotherapy is currently underway clinically based on the promising results of preclinical studies; multi-modal strategies to enhance antitumor efficacy *in vivo*, however, are essential for successful clinical outcome. In fact, most of the clinical trials for oncolytic viruses have been conducted in combination with chemotherapy or radiotherapy [80-83]. In a report of clinical trial of ONYX-015, no clinical benefit was noted in the majority of patients, despite the encouraging biological activity [84]. Tumor progression was rapid in most patients, even though substantial necrosis was noted in the tumors after treatment [85, 86]. Therefore, multi-disciplinary therapy composed of oncolytic virotherapy combined with low-dose chemotherapeutic agent is required to enhance the antitumor efficacy. Moreover, combination of two agents may allow the use of reduced dosage of each agent, and reduce the likelihood of adverse effects.

Infection with Telomelysin (GFP-expressing Telomelysin was used as an alternative to Telomelysin in some experiments) alone or followed by treatment with docetaxel (Taxotere), a chemotherapeutic agent, resulted in a profound *in vitro* cytotoxicity in various human cancer cell lines originating from different organs (lung, colon, esophagus, stomach, liver, and prostate), although the magnitude of antitumor effect varied among the cell types [77]. Other chemotherapeutic drugs such as vinorelbine (Navelbine) and SN38 (the potent active metabolite of irinotecan) combined with Telomelysin also inhibited the growth of human cancer cells [77]. Quantitative real-time PCR analysis demonstrated that docetaxel did not affect viral replication. For *in vivo* evaluation, mice xenografted with human lung tumor received intratumoral injection of Telomelysin and intraperitoneal administration of docetaxel. Analysis of growth of implanted tumors showed a significant, therapeutic synergism, while Telomelysin alone and docetaxel alone showed modest inhibition of tumor growth [77]. The antitumor effect of the combination therapy was likely additive *in vitro*; there might be, however, some particular interactions between Telomelysin and docetaxel to produce a synergistic effect *in vivo*. It has been reported that metronomic chemotherapy, which refers to long-term administration of comparatively low doses of cytotoxic drugs at close, regular intervals, has an antiangiogenic basis [87]. Like our approach, the potent antiangiogenic capacity of drugs administered in a metronomic fashion finds favor in a number of *in vivo* preclinical studies; to prove this efficacy by *in vitro* experiments is, however, technically difficult. There are some possible explanations for the superior *in vivo* antitumor activity in our experiments. Systemically administered docetaxel may attack the vascular endothelial cells at the tumor site, which in turn can block the escape of locally injected Telomelysin into the blood circulation. Another possibility is that Telomelysin itself may inhibit the vascular supply by killing endothelial cells.

FR901228 (depsipeptide, FK228) is a novel anticancer agent isolated from the fermentation broth of *Chromobacterium violaceum*. FR901228 has been identified as a potent histone deacetylase (HDAC) inhibitor. Histone deacetylation is an important component of transcriptional control, and it has been shown that FR901228 can increase Coxsackie's-adenovirus receptor (CAR) gene expression in various cancer cell lines [88-91]. Moreover, FR901228 is known to increase viral and transgene expression following adenovirus infection [88]. Indeed, FR901228 treatment upregulated CAR levels on target tumor cells, which in turn increased the amount of cellular Telomelysin replication, thereby promoting a synergistic antitumor effect [76]. These data indicate that FR901228 may be an appropriate partner for Telomelysin because it does not affect the virus life cycle. Delineating specific virus/drug combinations that are tailored to be particularly effective in human cancer could potentially improve the already encouraging results seen in the field of oncolytic virotherapy.

Clinical Application of Telomelysin

Preclinical models suggested that Telomelysin could selectively kill a variety of human cancer cells *in vitro* and *in vivo* via intracellular viral replication regulated by the hTERT transcriptional activity. Pharmacological and toxicological studies in mice and cotton rats demonstrated that none of the animals treated with Telomelysin showed signs of viral distress (e.g., ruffled fur, weight loss, lethargy, or agitation) or extensive histopathological changes in any organs at autopsy. These promising data led us to design a phase I clinical trial of Telomelysin as a monotherapy.

The proposed protocol "A phase I dose-escalation study of intratumoral injection with telomerase-specific replication-competent oncolytic adenovirus, Telomelysin (OBP-301) for various solid tumors" sponsored by Oncolys BioPharma, Inc. is an open-label, phase I, 3 cohort dose-escalation study. The Recombinant DNA Advisory Committee (RAC) at the National Institutes of Health (NIH) has already reviewed this protocol. The safety, tolerability, and feasibility of intratumoral injection of the agent will be assessed in patients with advanced cancer. The humoral immune response to Telomelysin will be analyzed also. Biopsies will be taken to evaluate the pharmacokinetics and pharmacodynamics of Telomelysin in the injected tumor. Therapeutic response will be assessed by measuring changes in tumor dimensions, comparative analysis of tumor biopsies, and cytokine and/or viral measurements. Patients selected for this trial have histologically or cytologically proven, non-resectable solid tumors and exhibited lack of response to conventional therapies such as primary external beam radiation or systemic chemotherapy. Patients have a disease that is measurable and accessible to direct injection of Telomelysin. Doses of Telomelysin will be escalated from low to high virus particles (VP) in one log increment. Patients will be treated with a single dose intratumoral injection of Telomelysin and then monitored for one month. The trial has been started upon approval of the US Food and Drug Administration (FDA) on November, 2006.

The data of pharmacokinetics and biodistribution of Telomelysin will be of interest. In the phase I trial of Advexin, a replication-deficient adenoviral vector that delivers normally functioning p53 tumor suppressor gene to cancer cells, the vector was present in tumor tissue as well as proximal lymph nodes, indicating regional spread of the vector via the lymphatic vessels [92]. Moreover, clinical trials of intratumoral and intravenous administration of CG7870, a replication-selective oncolytic adenovirus genetically engineered to replicate preferentially in prostate tissue, demonstrated a second peak of the virus genome in the plasma [93, 94], suggesting active viral replication and shedding into the bloodstream. Therefore, it is anticipated that intratumorally administered Telomelysin can spread into the lymphatic vessels as well as the blood circulation, and potentially kill metastatic tumor cells in regional lymph nodes and distant organ tissues. Theoretically, Telomelysin can replicate continuously in the injected tumors and releases virus particles unless all tumor cells are completely eliminated, indicating that a single intratumoral injection should be sufficient to induce antitumor effect. Our preclinical study, however, showed that multiple injections of Telomelysin resulted in a profound inhibition of tumor growth in xenograft models [74, 75, 77]. Thus, once the safety of a single administration is confirmed, the feasibility of the multi-cycle treatment with Telomelysin will be assessed in human.

hTERT PROMOTER FOR CANCER DIAGNOSTICS

Imaging of Tumor Cells using Telomelysin-GFP

A variety of imaging technologies is being investigated as tools for cancer diagnosis, detection, and treatment monitoring. Improvements in methods of external imaging such as computed tomography (CT), magnetic resonance imaging (MRI), and ultrasound techniques have increased the sensitivity for visualizing tumors and metastases in the body [95]; a limiting factor in structural and anatomical imaging, however, is the inability to specifically identify malignant tissues. Positron emission tomography (PET), with the glucose analogue ^{18}F-2-deoxy-D-glucose (FDG), is the first molecular imaging technique that was widely applied for cancer imaging in clinical settings [96]. Although FDG-PET has high detection sensitivity, it has some limitations such as difficulty in distinguishing between proliferating tumor cells and inflammation and unsuitability for real-time detection of tumor tissues. Therefore, tumor-specific imaging would be of considerable value in treatment of human cancer by defining the location and area of tumors without microscopic analysis. In particular, if tumors too small for direct visual detection and therefore not detectable by direct inspection could be imaged *in situ*, surgeons could precisely excise tumors with appropriate surgical margins. This paradigm requires an appropriate "marker" that can facilitate visualization of physiological or molecular events that occur in tumor cells but not normal cells.

The green fluorescent protein (GFP), which was originally obtained from the jellyfish *Aequorea Victoria*, is an attractive molecular marker for imaging in live tissues because of the relatively non-invasive nature of fluorescent [97]. A new approach developed in our laboratories to specifically visualize human tumor cells involves the use of Telomelysin and a replication-deficient adenovirus expressing the GFP gene (Ad-GFP) (Fig. **4**). Telomelysin infection could complement E1 gene functions and facilitate replication of E1-deleted Ad-GFP selectively in co-infected tumor cells [98]. When the human cancer cell lines were infected with Ad-GFP at low MOI, GFP expression could not be detected; in the presence of Telomelysin, however, Ad-GFP replicated in these tumor cells and showed strong green signals. By contrast, co-infection of Telomelysin and Ad-GFP did not show any fluorescence in normal cells such as fibroblasts and vascular endothelial cells because of the low levels of hTERT activity. This strategy was also applied successfully *in vivo*; intrathoracic administration of Telomelysin and Ad-GFP clearly labeled disseminated human lung tumor nodules in mice under the cooled charged-coupled device (CCD) camera (Fig. **4**). These data indicate that locoregional injection of Telomelysin plus Ad-GFP in combination with the highly sensitive CCD imaging system might be a useful diagnostic tool for real-time visualization of macroscopically invisible tumor tissues.

The advantage of co-infection of an E1-deleted replication-deficient adenoviral vector and Telomelysin is that transgene expression can be amplified in target cells. Furthermore, many vectors previously constructed can be used to express genes of interest. However, the requirement for both viruses to infect the same cell for the amplified transgene expression is a significant limitation of this dual virus vector system. The degree of

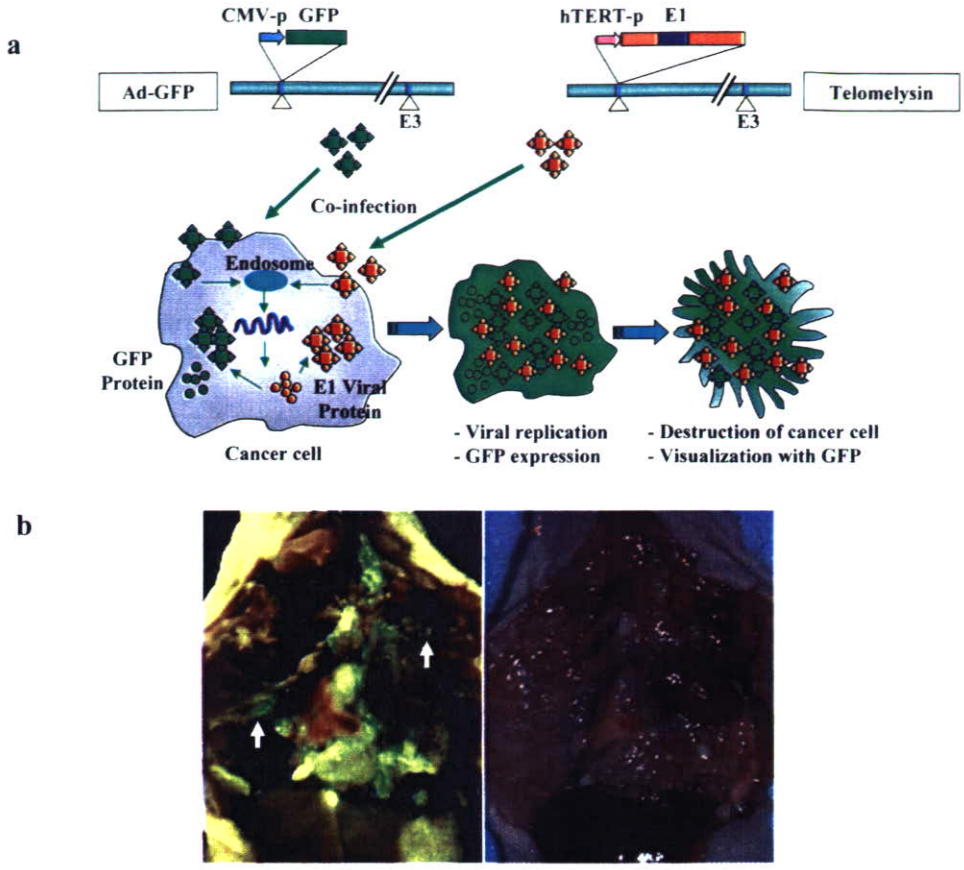

Fig. (4). (a) Concept of selective visualization of tumor cells with Ad-GFP and Telomelysin. **(b)** Internal images of pleural dissemination visualized by intrathoracic injection of Ad-GFP and Telomelysin. Female BALB/c *nu/nu* mice received intrathoracic implant with A549 human lung tumor cells. Five days after Ad-GFP and Telomelysin injection into the thoracic space, mice were sacrificed, and their thoracic spaces were examined. Fluorescent detection of disseminated tumors. *Arrows*, disseminated tiny tumor.

transgene expression has been shown to vary depending on the copy numbers of the viruses that initially infected the cells. To label efficiently and uniformly target tumor cells with green fluorescence, we modified Telomelysin to contain the GFP gene driven by the cytomegalovirus (CMV) promoter in the E3 deleted region (Fig. **2**). The resultant adenovirus was termed Telomelysin-GFP or OBP-401 [76, 77]. Similar to Telomelysin, Telomelysin-GFP replicated 5-6 logs by 3 days after infection in human cancer cell lines and coordinately induced GFP expression; Telomelysin-GFP replication, however, was attenuated up to 2 logs in normal human fibroblasts without GFP expression. Subcutaneous human tumor xenografts could be visualized after intratumoral injection of Telomelysin-GFP. Tumor sections entirely expressed GFP, suggesting *in vivo* viral replication and spread throughout the tumors.

In vivo Imaging of Metastatic Tumor Cells with Telomelysin-GFP

Metastatic spread of tumor cells plays a major role in the morbidity and mortality of human cancer. Although there are few life-prolonging treatments for the majority of patients with distant sites of metastasis, early detection of occult metastasis and early therapeutic interventions may decrease the rate of metastatic spread and extend survival. Lymphatic invasion is one of the major routes for cancer metastasis, and adequate resection of locoregional lymph nodes is required for curative treatment in patients with advanced malignancies. The risk of lymph node metastasis can be partially predicted by clinical data such as tumor stage, serum tumor marker level, and medical images; there are, however, no noninvasive approaches to accurately predict the presence of lymph node metastasis, in particular, microscopic metastasis. Although molecular analysis based on detection of genetic markers of cancer cells is clinically relevant in some patients, the procurement of sufficient tissue to confirm the diagnosis can be associated with significant morbidity and cost depending on the size and location of the lesion. Therefore, the utility of Telomelysin-GFP that can be used for real-time imaging of tumor tissues *in vivo* offers a practical, safe, and cost-effective alternative to the traditional, cumbersome procedures of histopathological examination.

Following intratumoral injection of Telomelysin-GFP into human colorectal tumors orthotopically implanted into the rectum in mice, para-aortic lymph node metastasis could be visualized at laparotomy under a CCD camera. Histopathological analysis confirmed the presence of metastatic adenocarcinoma cells in the lymph nodes with fluorescence emission, whereas GFP-negative lymph nodes contained no tumor cells. Of interest, metastatic lymph nodes were imaged in spots with GFP fluorescence, which was in agreement with histologically-confirmed micrometastasis. The sensitivity and specificity of this imaging technique are 92.3% and 86.6%,